

Original Article

Cite this article: Berke EH, Spry PG, Heimann A, Teale GS, Johnson B, von der Handt A, Alers B, and Shallow JM (2023) The genesis of metamorphosed Paleoproterozoic massive sulphide occurrences in central Colorado: geological, mineralogical and sulphur isotope constraints. *Geological Magazine* **160**: 1345–1375. <https://doi.org/10.1017/S0016756823000407>

Received: 1 February 2023

Revised: 16 June 2023

Accepted: 17 June 2023

First published online: 7 August 2023


Keywords:

regional metamorphism; Colorado; sulphur isotopes; mineralogy; volcanogenic massive sulphide deposits

Corresponding author: Paul G. Spry;

Email: pgspry@iastate.edu

The genesis of metamorphosed Paleoproterozoic massive sulphide occurrences in central Colorado: geological, mineralogical and sulphur isotope constraints

Edward H. Berke¹, Paul G. Spry¹ , Adriana Heimann², Graham S. Teale³, Benjamin Johnson¹, Anette von der Handt⁴, Brian Alers⁵ and John M. Shallow⁶

¹Department of Geological and Atmospheric Sciences, Iowa State University, 253 Science Hall, Ames, IA 50011-1027, USA; ²Department of Geological Sciences, East Carolina University, 101 Graham Building, East 5th Street, Greenville, NC 27858-4353, USA; ³Teale & Associates Pty Ltd, PO Box 740, North Adelaide, SA 5006, Australia; ⁴Department of Earth, Ocean and Atmospheric Sciences, University of British Columbia, 2020-2207 Main Mall, Vancouver, BC V6T 1Z4, Canada; ⁵Alers and Associates Limited, PO Box 775, Nederland, Colorado 80466, USA and ⁶JMS Geologic LLC, Boulder, CO, USA

Abstract

Paleoproterozoic massive Cu-Zn±Pb±Au±Ag sulphide deposits metamorphosed to the middle-upper amphibolite facies in central-south Colorado formed in a volcanic arc setting on the edge of the Yavapai crustal province. Previously published U-Pb ages on spatially related granitoids range from ~1.9 to ~1.1 Ga, while Pb isotope studies on galena from massive sulphides suggest mineralization formed at around 1.8–1.7 Ga. Some deposits in the Dawson-Green Mountain trend (DGMT) and the Gunnison belt are composed of Cu-Zn-Au-(Pb-Ag) mineralization that were overprinted by later Au-(Ag-Cu-Bi-Se-Te) mineralization. Sulphide mineralization is spatially related to amphibolite and bimodal, mafic-felsic volcanic rocks (gabbro, amphibolite, rhyolite and dacite) and granitoids, but it occurs mostly in biotite-garnet-quartz±sillimanite±cordierite schists and gneisses, spatially related to nodular sillimanite rocks, and in some locations, exhalative rocks (iron formations, gahnite-rich rocks and quartz-garnetite). The major metallic minerals of the massive sulphides include chalcopyrite, sphalerite, pyrite, pyrrhotite, and magnetite, with minor galena and gahnite. Altered rocks intimately associated with mineralization primarily consist of various amphiboles (gedrite, tremolite and hornblende), gahnite, biotite, garnet, cordierite, carbonate and rare högbomite. The Zn/Cd ratios of sphalerite (44 to 307) in deposits in the DGMT fall within the range of global volcanogenic massive sulphide (VMS) deposits but overlap with sphalerite from sedimentary exhalative (Sedex) deposits. Sulphur isotope values of sulphides ($\delta^{34}\text{S} = -3.3$ to $+6.5$) suggest sulphur was largely derived from magmatic sources, and that variations in isotopic values resulting from thermochemical sulphate reduction are due to small differences in physicochemical conditions. The preferred genetic model is for the deposits to be bimodal-mafic (Gunnison) to mafic-siliciclastic VMS deposits (Cotopaxi, Cinderella-Bon Ton, DGMT).

1. Introduction

The Paleoproterozoic era (2.5–1.6 Ga) represents a period in Earth's history when some of the world's largest volcanogenic massive sulphide (VMS), sedimentary exhalative (Sedex), Bergslagen-type bedded, stratiform Zn-Pb-Ag mineralization hosted in rhyolitic ash-siltstone (SAS-type)/stratabound volcanic-associated, limestone-skarn (SVALS-type) and Broken Hill-type (BHT) deposits formed (e.g. Flin Flon-Snow lake VMS deposit, Gibson *et al.* 2013; Broken Hill Pb-Zn-Ag deposit, Parr & Plimer, 1993; Lappbergert SVALS-type Zn-Pb-Ag-(Cu-Au) deposit, Tiu *et al.* 2021; Rampura Agucha Zn-Pb-Ag Sedex deposit, Mishra & Bernhardt, 2009).

In the United States, Paleoproterozoic massive sulphide deposits include VMS deposits in the ~1.81 Ga Penokean Volcanic Belt, Wisconsin (e.g. Moleski *et al.* 2019), the largest of which is Crandon (42.9 Mt @ 0.6% Cu, 8.4% Zn, 51 g/t Ag and 1.4 g/t Au), as well as those in the ~1.74 Ga Jerome VMS district (>100 Mt of Cu-Zn-Pb-Ag), Arizona, and the ~1.8 to 1.7 Ga massive sulphide belt in south-central Colorado. Massive sulphide deposits in Arizona and Colorado occur in the regional Yavapai tectonic terrane, or the transitional Yavapai–Mazatzal tectonic terrane, that extends from Nevada through to Colorado. The impetus for the study was, in part, based on the observations of Karlstrom *et al.* (1999) and Burrett and Berry (2000) who placed North America adjacent to Australia in the Neoproterozoic supercontinent Rodinia. Such a tectonic reconstruction means that the Willyama Complex in Australia, which contains the supergiant Broken Hill deposit (280 Mt of 10.0% Pb, 8.5% Zn and 148 g/t Ag, Parr & Plimer,

© The Author(s), 2023. Published by Cambridge University Press. This is an Open Access article, distributed under the terms of the Creative Commons Attribution licence (<http://creativecommons.org/licenses/by/4.0/>), which permits unrestricted re-use, distribution and reproduction, provided the original article is properly cited.



1993; Spry & Teale, 2021), connects with the Yavapai belt. Given the enormous size of Broken Hill and the Jerome district, the Paleoproterozoic of Colorado is considered to have potential for the presence of large massive sulphide deposits.

While the aforementioned deposits in Wisconsin and Arizona are unmetamorphosed or were metamorphosed to the lower greenschist facies, some small deposits in Arizona (e.g. Antler and Copper World Cu-Zn-Pb VMS deposits in the Hualapai Mountains; Stensrud & More, 1980; Donnelly *et al.* 1987) were metamorphosed to the middle amphibolite facies. Here, we evaluate the genesis of small metamorphosed massive sulphide deposits in south-central Colorado, the largest of which is Sedalia (1.25 Mt @ 3.3% Cu, 5.6% Zn, 23 g/t Ag and 0.3 g/t Au; Heinrich, 1981). Previous genetic models for the formation of these deposits have been the subject of debate and include VMS (e.g. Drobeck, 1981; Sheridan & Raymond, 1984a; Alers & Shallow, 1996; Shallow & Alers, 1996), carbonate-replacement skarn (e.g. Salotti, 1965), BHT (Zephyr Minerals Limited, 2018; <https://www.zephyrminerals.com/dawson-section>), and most recently, high-temperature fractionation of base and precious metals from peraluminous granitoids (Kleinhans & Swan, 2022).

Although more than 20 Paleoproterozoic sulphide occurrences were identified by Sheridan and Raymond (1984a) in north-central and south-central Colorado, we primarily focus, from west to east, on the Vulcan-Good Hope, Cinderella, Cotopaxi, Green Mountain, El Plomo, Horseshoe, and Dawson deposits. The last four deposits occur in a linear belt near Cañon City that we refer to as the Dawson-Green Mountain trend (DGMT). In this contribution, we evaluate the geological setting along with the major and trace element studies of various rock types (including metamorphosed hydrothermally altered rocks and granitoids), the compositions of minerals in the sulphide-bearing units and attendant alteration, and the sulphur isotope ratios of sulphides in various deposits. The present contribution complements previous studies on aspects of the geology of these occurrences, including the descriptive geology of the deposits by Sheridan and Raymond (1984a, 1984b), the genetic relationship of garnite to sulphide mineralization (Heimann *et al.* 2005), the origin of gedrite-garnet-cordierite rocks at the Evergreen prospect (Heimann *et al.* 2006), and the genetic relationship of nodular sillimanite rocks to sulphide mineralization (Spry *et al.* 2022b). The aim of the current study is to evaluate the origin of the various deposits and to provide exploration tools that can potentially be used as guides to further mineralization in regionally metamorphosed rocks in south-central Colorado.

2. Regional geology

The central-southwestern part of the United States is dominated by four crustal terranes/provinces: Wyoming, Mojave, Yavapai and Mazatzal, the first of which is Archean in age (c. 3.5–2.5 Ga; Shaw & Karlstrom, 1999; Jones *et al.* 2010) while the other three provinces are of Proterozoic age and were accreted onto the margin of the Wyoming province. Metamorphosed massive Cu-Zn-Au-(Pb-Ag) deposits extend in a discontinuous belt from the Wet Mountains, in central southern Colorado, to the Independence Mountains, near the Colorado-Wyoming border in a package of metasedimentary, granitoids and bimodal metavolcanic rocks (Fig. 1). These deposits primarily occur in the Yavapai province and the so-called “transition zone” that is ~ 300 km wide and occurs between the Yavapai and Mazatzal provinces (Fig. 2). The Yavapai province is a coalescence of juvenile arc terranes that formed around 2.0–1.8 Ga, while the Mazatzal Province, with a Nd

model age of ~1.8–1.7 Ga (Bennet & DePaolo, 1987), is considered to be a microcontinent that was accreted onto the southern margin of the Yavapai province during the Mazatzal orogeny at around 1.65–1.60 Ga (Condie, 1982; Karlstrom, 1998; Karlstrom & Humphreys, 1998; Anderson & Cullers, 1999; Whitmeyer & Karlstrom, 2007; Grambling *et al.* 2015). The transition zone marks the location of the Yavapai–Mazatzal suture and is characterized by strong deformation (Karlstrom, 1998; Karlstrom & Humphreys 1998; Shaw & Karlstrom, 1999). Extensional tectonic regimes are associated with terrane accretion and the development of ductile shear zones. The study area is characterized by isoclinal folds, while the second and third deformation events formed large open folds. The major structures generally trend northwest to north.

Granitoids are widespread throughout the Proterozoic terrane in Colorado and were emplaced from 1.9 to 1.1 Ga during three episodes (e.g. Bickford *et al.* 1989; Anderson & Cullers, 1999; Siddoway *et al.* 2000). Major Paleoproterozoic calc-alkaline granitoids were intruded at 1.9 to 1.7 Ga granitic with more peraluminous plutons occurring at ~1.7 Ga (Anderson & Cullers, 1999; Premo & Fanning, 2000). Granitic plutonism subsequently occurred at ~ 1.45 to 1.35 Ga with the emplacement of A-type granitic batholiths (e.g. Peterman *et al.* 1968) followed by a later period of A-type intrusions (or ferroan granitoids using the terminology of Frost & Frost, 2011), which was associated with the formation of the Pikes Peak batholith at around 1.1 Ga (Hedge, 1970). Metamorphosed massive sulphide deposits are spatially associated with the first generation of granitoid emplacement around the Gunnison and Salida areas (Sheridan & Raymond, 1984a, 1984b), while the ages of those spatially associated with deposits in the DGMT are unknown due to the absence of geochronological studies. Nonetheless, Pb-Pb isotope ages of galena that were analysed by Bruce Doe in the 1970s and reported in Sheridan and Raymond (1984a, 1984b) suggest that sulphide mineralization formed between 1.8 and 1.7 Ga. Z. Palmer (unpub. M.S. thesis, Colorado School of Mines, 2019) showed that the small Isabel and Amethyst Cu-Zn deposits in the southern Wet Mountains were spatially and genetically associated with the A-type San Isabel granite (U-Pb age of monazite of 1.37 to 1.13 Ga) and are younger than the other metamorphosed massive sulphide deposits in Colorado.

Rocks in central-southern Colorado were mostly metamorphosed to the middle to upper amphibolite facies, similar to the metamorphic grade observed in Proterozoic rocks of northern Colorado and New Mexico (e.g. Pedrick *et al.* 1998; Shaw & Karlstrom, 1999). However, upper greenschist–lower amphibolite facies conditions were reported by Sheridan *et al.* (1981) for the Gunnison district in the west, while upper amphibolite–granulite facies conditions occur in the southern Wet Mountains spatially associated with the Isabel and Amethyst deposits (Sheridan & Raymond, 1984b). Steep gradients between greenschist to upper amphibolite conditions occur in localized areas (e.g. 25 km west of Cañon City; Shaw & Karlstrom, 1999, Fig. 2, p. 42) and is likely related to pluton-enhanced metamorphism and possible composite effects of superimposed metamorphic events. Although conditions mostly reflect regional metamorphism associated with the Yavapai orogeny (the Colorado orogeny of Sims & Stein, 2003 at 1.78 to 1.69 Ga), localized reheating and superimposed metamorphism (primarily to the amphibolite facies) is also associated with the Mazatzal orogeny (the Berthoud orogeny of Sims & Stein, 2003) at ~ 1.45 to 1.35 Ga (e.g. Möller *et al.* 2022).

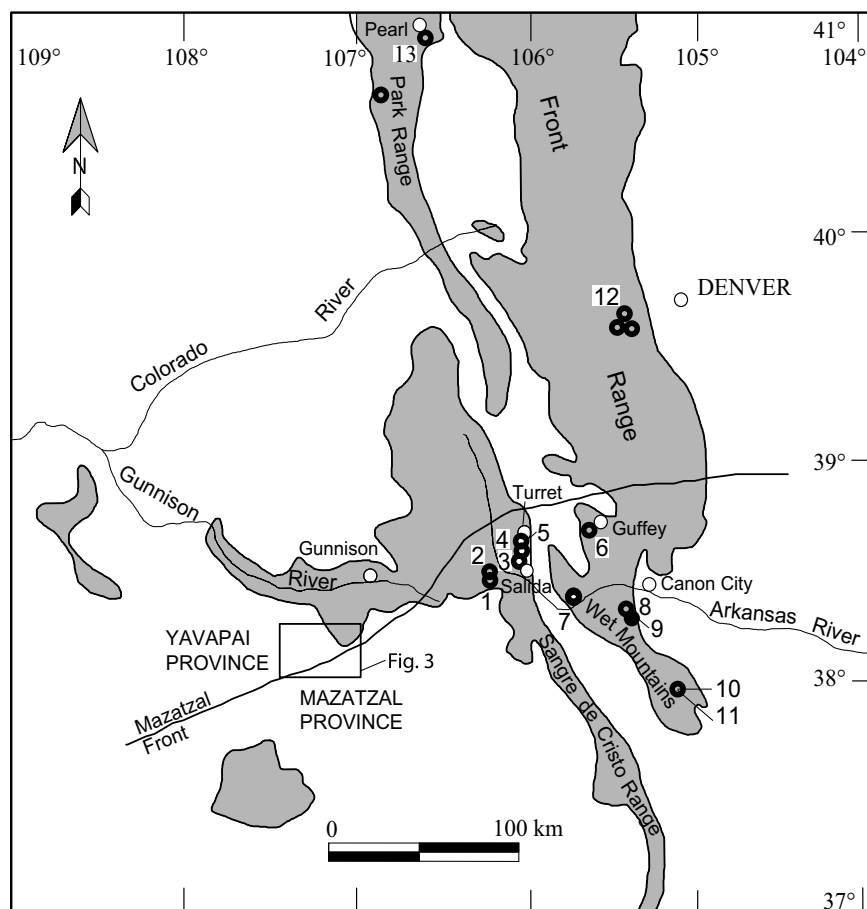


Figure 1. (Colour online) General map of Colorado showing the extent of Proterozoic rocks (grey shaded pattern; after Sheridan and Raymond, 1984), terrane boundaries (after Shaw and Karlstrom, 1999), and location of metamorphosed massive sulphide deposits: 1 Bon Ton, 2 Cinderella, 3 Sedalia, 4 Ace High/Jackpot, 5 Independence, 6 Betty (Lone Chimney), 7 Cotopaxi, 8 Green Mountain, 9 Dawson-Grape Creek trend, 10 Marion, 11 Amethyst, 12 Evergreen hydrothermal alteration zone, Cresswell, F.M.D., and Hosa Lodge, and 13: Caprock. The location of the Mazatzal Deformation Front is derived from Shaw and Karlstrom (1999). Figs. 2, 3 are shown as insets.

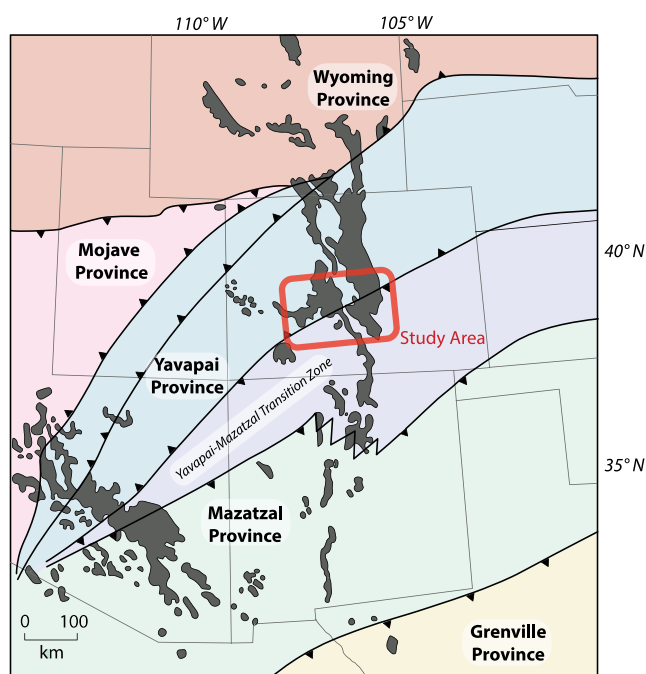


Figure 2. (Colour online) Regional geologic map of the southwestern United States. Major crustal provinces, transition zones, inferred boundaries and deformation fronts are also delineated (modified after Jones *et al.* 2010). An inset map showing the study area (see Fig. 1) is also indicated.

3. Analytical methods

3.a. Whole rock analyses

Most bulk rock compositions of samples ($n = 53$) were analysed by Bureau Veritas, Vancouver, British Columbia using analytical package LF202. Major oxides ($n = 11$), loss-on-ignition, and the following trace elements (Ag, As, Au, Ba, Be, Bi, Cd, Co, Cs, Cu, Ga, Hf, Hg, Mo, Nb, Ni, Pb, Rb, Sb, Sc, Se, Sn, Sr, Ta, Th, Tl, U, V, W, Y, Zn and Zr; plus the rare earth elements (REEs) (Ce, Dy, Er, Eu, Gd, Ho, La, Lu, Nd, Pr, Sm, Tb, Tm and Yb) were prepared by lithium borate fusion and analysed by inductively coupled plasma-atomic emission spectroscopy (ICP-AES)/inductively coupled plasma mass spectrometry (ICP-MS) and X-ray fluorescence techniques. The detection limits for the oxides are 0.01 wt.%, except for Cr_2O_3 , which is 0.002 wt.%, while those for most of the trace elements using this technique, but not including the REEs, range from 0.1 to 0.5 ppm, except for Ba, Be and Sc, which have detection limits of 1 ppm. The detection limits for Ni and Sn are 20 and 8 ppm, respectively, while the REEs have detection limits ranging from 0.01 to 0.1 ppm. Total sulphur and carbon were analysed with a Leco instrument, with detection limits of 0.02 wt.%. The following trace elements Ag, As, Au, Bi, Cd, Cu, Hg, Mo, Ni, Pb, Sb, Se, Tl and Zn were digested in aqua-regia and analysed by ICP-AES and ICP-MS techniques. The detection limits for these elements varied from 0.1 to 1 ppm, depending on the element.

Fifteen samples were analysed by Actlabs, Ancaster, Ontario. Major oxides ($n = 11$) plus the same trace elements noted above

except, for Cr, Hg and Sc, were analysed by ICP-optical emission spectrometry, instrumental neutron activation and ICP-MS. Sample fusion employed a lithium metaborate/tetraborate technique. The detection limits for the oxides are 0.01 wt.%, except for MnO and TiO₂, which are 0.001 wt.%. REEs had detection limits of 0.005 to 0.1 ppm, while the remainder of the elements have the following detection limits: Bi (0.4 ppm), Ag, Cs, and Sb (0.5 ppm), Be, Co, Ga, Ge, Nb, Sc, Sn, W, and Y (1 ppm), Mo, Rb, Sr, and Zr (2 ppm), As, Pb, and V (5 ppm), Cu (10 ppm), and Zn (30 ppm).

3.b. Electron microprobe analyses

Samples were studied petrographically, and the compositions of silicates and oxides were obtained using an ARL-SEM-Q electron microprobe in the Department of Geological and Atmospheric Sciences at Iowa State University and a JEOL JXA-8530FPlus Electron Probe Microanalyzer at the University of Minnesota. Analyses of silicates for both electron microprobes were conducted using a 15-kV accelerating voltage with a 20-nA beam current, a 1–2 μm spot size. Mineral standards included hornblende (Si, Al, Mg and Ca), ilmenite (Ti, Fe), albite (Al, Na), spessartine (Al, Mn), pyrope (Si, Mg), K-feldspar (K), gahnite (Zn, Al), tugtupite (Cl) and apatite (F). Quantitative analyses of sulphides were obtained under two sets of conditions for the analyses of sphalerite from the Vulcan, Horseshoe, El Plomo, and Dawson deposits to determine Zn/Cd ratios and for the analyses of galena, pyrrhotite, and argentopyrite from the Horseshoe and El Plomo deposits. Both sets of analyses were performed at the University of Minnesota with the samples of sphalerite for the determination of Zn/Cd ratios using the following analytical conditions: an accelerating voltage of 15 kV, a beam current of 50 nA and a beam diameter of 5 microns. Element compositions were acquired using analysing crystals LIFL for Zn α , Mn α , Fe α , Cu α , PETL for Cd α , and PETJ for S α and Ag α . The standards were Mn-olivine and synthetic and Mn₂SiO₄ for Mn, Cu metal for Cu, pyrite for Fe, sphalerite for Zn and S, hessite for Ag, and cadmium sulphide (CdS) for Cd. The on-peak counting time was 10 seconds for Zn α , Mn α , Fe α , Cu α , S α , 40 seconds for Ag α and 60 seconds for Cd α . The analyses of sulphides from the Horseshoe and El Plomo deposits used the same operating conditions but also analysed for Pb, As, Se, Sb, Au and Bi, using the following standards: galena for Pb and S, sphalerite for Zn and S, indium arsenide for As, as well as native metals for Ag, Au, Bi, Sb and Se. The on-peak counting time was 10 seconds for all elements. The mean atomic number (MAN) background intensity method was used instead of the traditional off-peak background acquisition (Donovan & Tingle, 1996; Donovan *et al.* 2016). The MAN background intensity data were calibrated, and continuum absorption corrected for Cd α , Zn α , Mn α , Fe α , Cu α , S α and Ag α . Unknown and standard intensities were corrected for dead time. The Phi-Rho-Z matrix correction algorithm Armstrong/Love Scott (CitZAF) was used along with the mass absorption coefficients dataset FFAST (Chantler *et al.* 2005).

3.c. Scanning electron microscopy

Images and energy-dispersive X-ray spectroscopy (EDS) point analyses of sulphides and sulphosalts were obtained on a JEOL JSM-IT100 InTouch scanning electron microscope (SEM) using the backscatter electron composition (BED-C) mode at Iowa State University. The probe current ranged between 65 and 75 nA with a low vacuum pressure of approximately 100 Pa and an accelerating voltage of 10–20 kV.

3.d. Sulphur isotope analyses

Pyrite, pyrrhotite, chalcopyrite and sphalerite were separated from samples by hand-picking under a binocular microscope or were drilled out using a Dremel tool with a 1-mm drill tip. We followed the procedure for sulphur isotope analysis as described by Grassineau (2006) and Spry *et al.* (2022a). The mineral concentrates were pulverized in an agate mortar to a powder, which weighed between ~0.75 and 3.0 mg depending on the composition of the sulphide (chalcopyrite: ~1.5 mg, galena: ~3.0 mg, pyrite: ~0.75 mg and pyrrhotite ~0.75 mg, sphalerite ~1.5 mg). The powder was loaded into tin capsules and burned using a Thermo Scientific Flash IRMS IsoLink elemental analyser. The tin capsules were oxidized at ~1020 °C and when oxygen was added it flash combusted at 1800 °C (Grassineau, 2006). The oxygen was added at a rate of 300 ml/minute for 3 seconds. The SO₂ gas produced was purified through a gas chromatography column and then introduced via a ConFlo IV Universal Interface system into a continuous flow-type dual-inlet ThermoScientific Delta V Series Isotope Ratio mass spectrometer under He flow. The analysis time was ~ 420 seconds. The $\delta^{34}\text{S}_{\text{VCDT}}$ values were calculated using calibration curves obtained for seven internal standards obtained from the Queen's Facility for Isotope Research (QFIR) at Queen's University, Canada, and two internal standards provided by Thermo Scientific (see Spry *et al.* 2022a). These standards are Q-GEMA pyrite = +3.0‰, NBS IAEA-SO-6 barite = -34.1‰, 127 barite = +20.3‰ ($\pm 0.3\%$), IAEA-SO-5 barite = +0.5‰, MRC pyrite = +0.7‰, QFIR pyrite = -0.5‰, M6801 barite = +12.5‰, and peat = -13.15‰ ($\pm 0.3\%$), and sulphanilimide = -1.24‰ ($\pm 0.2\%$). The isotopic values of the standards are relative to the internationally recognized sulphur isotope standard Cañon Diablo troilite (FeS). The analytical precision of the data is $\pm 0.1\%$.

4. Local geology of mineral deposits

Although samples were obtained from over 15 massive sulphide prospects, the focus here is on the low metamorphic grade Vulcan-Good Hope deposits (upper greenschist–lower amphibolite facies) to potentially see through the camouflaging effects of metamorphism and associated deformation, as well as the Cinderella-Bon Ton and Cotopaxi deposits and those that are currently the subject of recent exploration activity along the DGMT (Green Mountain, El Plomo, Horseshoe, Dawson), which were metamorphosed to the upper amphibolite facies. The geological characteristics of the massive sulphide deposits are in Table 1. Although nodular sillimanite rocks and gahnite-bearing rocks are spatially associated with several deposits listed in Table 1, they were the focus of studies by Spry *et al.* (2022b) and Heimann *et al.* (2005), respectively, and will only be discussed here as they relate to the origin of the deposits and their potential as exploration guides to metallic mineralization. Note we use the term 'gahnite' here for zinc-bearing spinels regardless of the Zn-Fe-Mg proportion, which was shown by Heimann *et al.* (2005) to be variable in composition for deposits in Colorado.

4.a. Vulcan-Good Hope

The Vulcan-Good Hope deposits, which extend for a distance of ~500 m, were the largest gold producers in the Dubois Greenstone Belt and likely part of the same hydrothermal system. The belt consists of clastic sediments, andesite to basalt flows and tuffs, rhyolite, and chert metamorphosed to the upper greenschist–lower

Table 1. Summary of geological characteristics of selected metamorphosed massive sulphide deposits, Colorado

Deposit	Grades, reserves, past production and metallic minerals	Country rocks	Mineralized and metamorphosed altered rocks	References
Ace High/Jackpot*	Unknown grade, best sample from dump: >10% Cu, 0.4% Zn, 198 g/t Ag, Ccp, Sp, Mag	Bt-Qz gneiss, amphibolite, Bt schist, nodular Sil schist	Nodular Sil-Grt schist, Ghn-Phl-Ms-Chl gneiss, Grt-Bt-Py gneiss, Mag-Hbl gneiss, Ath-Ghn schist, Crd-Ath-Ghn-Ms rock; Cum-Ghn rock; Ath-Crd-Ghn-Phl rock	Van Alstine (1969), Boardman (1986)
Amethyst*	Unknown production, Sp, Ccp, Gn, Py, Pyh	Amp-Bt gneiss, granite	Spr-Amp rock, Spl-Amp rock, Spr-Spl-Bt-Crn rock, Spr-Crd-pl-Spl rock, Spr-Crd-Spl-Bt rock	Raymond <i>et al.</i> (1980)
Betty (Lone Chimney)*	Past production: 3,900 kg Cu, 1,680 kg Pb, 1,680 kg Zn, 4.76 kg Ag, 312g Au, Py, Ccp, Sp, Gn, Pyh, Py, Bn, Cv, Ilm, Mag, Hem	Bt gneiss, Qz-Ms schist, Qz-Crd-Sil gneiss, amphibolite	Qz-Crd-Sil gneiss, nodular Sil gneiss, Calc-silicate gneiss, Crd-Ath rock, Ghn rock, Act-Bt rock, Ath rock, Qz-Crd rock	Heinrich (1981)
Bon Ton*	Unknown grade, best sample from dump: 1.9% Cu, 6.4% Zn, 47 g/t Ag, Sp, Py, Ccp, Pyh,	Fsp-Bt-Qz-Ep gneiss, amphibolite, feldspathic quartzite, Qz-Fsp-Ms-Sil gneiss, Bt-Qz-Fsp-Hbl gneiss, Qz-Fsp-Bt gneiss	Nodular Sil gneiss, iron formation, Bt-Grt schist, quartzite, Ms schist; Grt-Bt-Crd-Qz-Ghn-sulphide rock; Ghn-Bt rock; Phl-Qz-sulphide rock	D.C. Knight (unpub. MS thesis, Univ. Manitoba, Winnipeg, 1981)
Caprock*	0.9 Mt of 8% (Zn+Pb) projected reserves; Sp, Gn, Py, Pyh	Qz-Fsp-Sil-Grt-Bt gneiss, nodular Bt-Sil-Qz-gneiss	Ghn-Grt-Bt rock, nodular Sil-Ms rock, Ath-Cum-Ol-Ghn-Crd rock	P.D. Klipfel (unpub. PhD thesis, Colorado School of Mines, Golden, 1992)
Cinderella*	Unknown grade, best sample from dump: 1.9% Cu, 6.4% Zn 47 g/t Ag; Sp, Ccp, Gn, Py,	Sil-Qz-Ms gneiss, Qz-Bt-Ep gneiss, amphibolite, Grt gneiss	Nodular Sil rock, Bt-Grt schist, Bt gneiss, Ms schist, Ath-Crd rock, quartzite, Ghn-Ath-Crd-Phl-Tr rock, Phl-Qz-Grt-Ghn-Chl rock, Rdn-Act-Qz rock	Heinrich (1981)
Cotopaxi*	Past production: 0.01 of 1,337 tonnes Zn, 83 tonnes Cu, 71 tonnes Pb, 301 kg Ag, 4.5 kg Au; Sp, Ccp, Gn, Pyh, Py, Mrc, Rt, Ilm, Mol, Cv, Mag	Qz-Bt-Fsp-Sil gneiss, nodular Sil schist, Hbl gneiss, Bt schist, calc-silicate gneiss, granite gneiss, pegmatite	Nodular Sil-Bt rock, Ath-Bt gneiss, Ghn-Qz-Grt rock, pegmatitic Ghn-Bt rock, Chl schist, Qz-Bt garnetite, Ath-Phl-Crd-Ghn rock, Act-Fo-Ghn-Ccp-Gn-Sp rock, Cum-Qz-Bt-Ms rock	Lindgren (1908), Salotti (1965)
Dawson*	No production, ~4,250 kg Au @ 5g/t; Py, Pyh, Ccp, Sp, Mag, Ghn	Granite gneiss, Bt schist, Qz-Bt-Grt gneiss, amphibolite, metagabbro, pegmatite	Qz-Bt±Grt gneiss, Fsp-Bt-Mag-Qz gneiss, Qz-Bt-Sil gneiss, Bt-Grt-Ath-Crd±Ghn±Hbl±Tr-Mag rock, Ath-Chl-Bt-Tlc-Srp-Qz rock	Berke <i>et al.</i> (2022), Kleinhans and Swann (2022)
El Plomo*	Best drill hole intersections: 9.2% Pb and 0.7% Cu over 1.6 m and 4.6% Zn, 0.2% Cu, and 0.2 % Pb over 1.5 m; Py, Pyh, Sp, Gn, Ccp, Mag, Ghn	Qz-Fsp-Bt±Crd±Sil±Grt rock, amphibolite, granite gneiss, Bt-Qz monzodiorite	Qz-Ath-Crd-Bt rock, Qz-Bt-Chl-Ksp gneiss, Ath-Crd-Ghn-Bt-Py-Po-Ccp-Gn-Sp rock	Unpub. US Borax report, 1981 drilling results, Grape Creek project, Fremont County, Colorado
Evergreen*	No production, Ccp, Sp, Pyh	Sil-Ms-Qz-Alm gneiss, Ged-Alm-Crd gneiss, amphibolite, calc-silicate rock	Ged-Alm-Crd gneiss, nodular Sil rock	Heimann <i>et al.</i> (2006)
Independence*	Unknown grade but best sample from dump: 3.3% Cu, 1.3% Zn, 1.8 g/t Ag; Ccp, Sp, Pyh, Py, Cv, Mol, Ilm, Mag	Bt-Qz gneiss, granite, amphibolite, pegmatite, Bt-Ms schist	Ghn-Crd-Ath rock, nodular Sil rock; Phl-Ghn-Chl-sulphide rock; Qz-Sil-Crd-St-Grt-Ghn rock	Lindgren (1908) Heinrich (1981)
Green Mountain*	Best drill hole intersection: 18.1 % Cu and 4.3 % Zn over 1.5 m; Ccp, Py, Sp, Gn, Mol, Pyh, Ilm, Hem, Rt	Qz-Fsp gneiss, Qz-Crd-Grt-Bt gneiss, migmatite, Ath-Crd rock, nodular Sil rock, Sil gneiss, Hbl-Bt-Crd gneiss, amphibolite	Nodular Sil rock, Qz-Grt gneiss, Ath-Crd-Ghn rock, Grt amphibolite, Grt-Sil gneiss, Qz-garnetite, Qz-Bt gneiss, Grt-bearing pegmatite, Ath-Crd-Cum-Ghn-Grt rock, gabbro	G.T. Ririe (unpub. PhD thesis, Univ Iowa, 1981);the present study
Horseshoe*	Best drill hole intersection: 4.4% Zn over 3 m; Sp, Gn, Ccp, Mag, Ghn, Po	Qz-Fsp-Bt-Crd gneiss, migmatite, amphibolite, granite gneiss, monzodiorite	Qz-Bt gneiss, Ath-Crd-Ghn-Bt-Py-Po-Ccp-Sp rock	The present study
Marion*	Unknown production; Sp, Ccp, Gn, Py, Pyh, Py, Mrc, Mol, Bn, Mag, Rt	Amp-bearing gneiss, calc-silicate gneiss, impure marble, granite, migmatite	Spr-Ath-Spl-Bt rock, Ged-En-Crd-Spl rock	Heinrich (1981), Raymond <i>et al.</i> (1980)

(Continued)

Table 1. (Continued)

Deposit	Grades, reserves, past production and metallic minerals	Country rocks	Mineralized and metamorphosed altered rocks	References
Sedalia*	1.2 Mt @ 3.2% Cu, 5.6% Zn, 23 g/t Ag, 0.28g/t Au; Sp, Ccp, Gn, Cv, Py, Mrc, Pyh, Mag, Ghn, Ilm, Native Au, Native Ag	Feldspathic gneiss, Bt-Ms schist, amphibolite, Grt-Crd amphibole gneiss, Grt-Bt schist, pegmatite	Crd-Ath-Sil-Grt gneiss, And-rich rock, Mag-Chl-Alm rock, Hbl-Ep-Qz-Sil-Pl rock, Act rock, Tr-Pl rock, Tr-Chl rock	Lindgren (1908), Heinrich (1981) D.C. Knight (unpub. MS thesis, Univ. Manitoba, Winnipeg, 1981)
Vulcan-Good Hope**	700 kg of Au; Py, Pyh, Sp, various Te-bearing minerals, tertiary Au overprint	Rhyolite tuff, basalt-andesite flows, granite, trachyte dike	Qz-Ser schist, Qtz-Chl schist, Qz-Ser-Chl rock	Drobeck (1981), Sheridan <i>et al.</i> (1981), Hartley (1983)

Abbreviations after Warr (2021);

*Metamorphosed to the upper amphibolite facies;

**Metamorphosed to the upper greenschist-lower amphibolite facies.

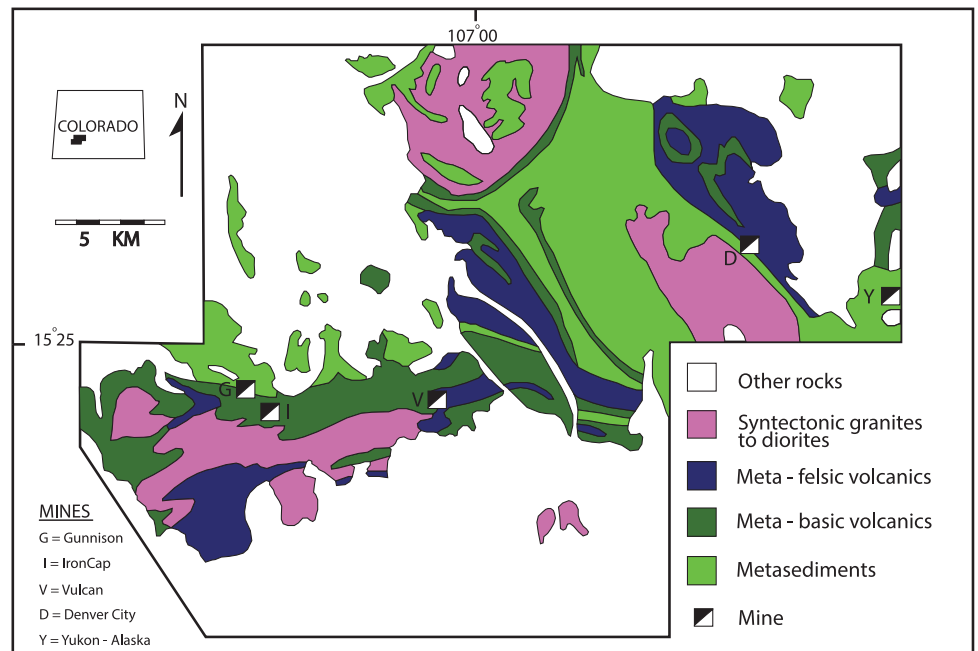


Figure 3. (Colour online) Geological map of the Gunnison district showing the location of the Vulcan-Good Hope deposits (V), along with the Gunnison (G), Iron Cap (I), Denver City (D) and Yukon-Alaska (Y) deposits (modified after Drobeck 1981).

amphibolite facies along with syn- and post-tectonic granitoids (Drobeck, 1981; Sheridan *et al.* 1981; Hartley, 1983) (Fig. 3). The deposits occur in felsic metavolcanic rocks, which Drobeck (1981) interpreted as dacite to rhyolite flows, tuffs and tuffaceous sediments interleaved with metabasalt and meta-andesite. Metamorphosed sediments (greywackes, siltites and argillites) are also locally present as is magnetite-bearing quartzite, which occurs along strike from the sulphide zone. The deposits are conformable to sedimentary layering and surrounded by an envelope of quartz-sericite pyrite alteration (Fig. 4a), which in turn is surrounded by a halo of quartz-chlorite alteration (Drobeck, 1981). The dominant sulphides are pyrite, pyrrhotite and sphalerite (Fig. 4b), with chalcopyrite, arsenopyrite and galena occurring in minor amounts. The sulphides show crude banding parallel to the conformable schistosity and sedimentary layering. Of note is the presence of a superimposed Au-Ag-Te-S-Sb-Bi-As-Hg-Se system on the massive sulphides which Drobeck (1981) suggested may have formed during the Miocene. However, timing relationships are unclear, and it is possible that this

superimposition occurred during the Proterozoic. The overprinted mineralization is dominated by tellurium-bearing species in chalcidonic veinlets, which consist of native Te crystals, tellurite, coloradoite, tetradymite, tellurobismutite, petzite, sylvanite and frobergite. The Vulcan-Good Hope system is the type locality for the relatively rare Cu tellurides (rickardite, weissite, cameronite, spirodonite and vulcanite) and zincmelantherite (Eckel, 1961; Cameron & Threadgold, 1961; Drobeck, 1981; Hartley, 1983).

4.b. Cinderella-Bon Ton

The Cinderella deposit consists of Zn-Cu±Pb mineralization and is located 2 km south and along strike from the Bon Ton deposit (D.C. Knight, unpub. MSc thesis, Univ. Manitoba, 1981) (Fig. 5). The Cinderella deposit occurs on the south-east limb of a northeasterly plunging fold, whereas the Bon Ton deposit occurs at the closure of the fold. Isoclinal folds near the Cinderella deposit are evident. The Boulder Creek granite crops out 1.6 to 3.2 km west-northwest of the mineralized horizon.

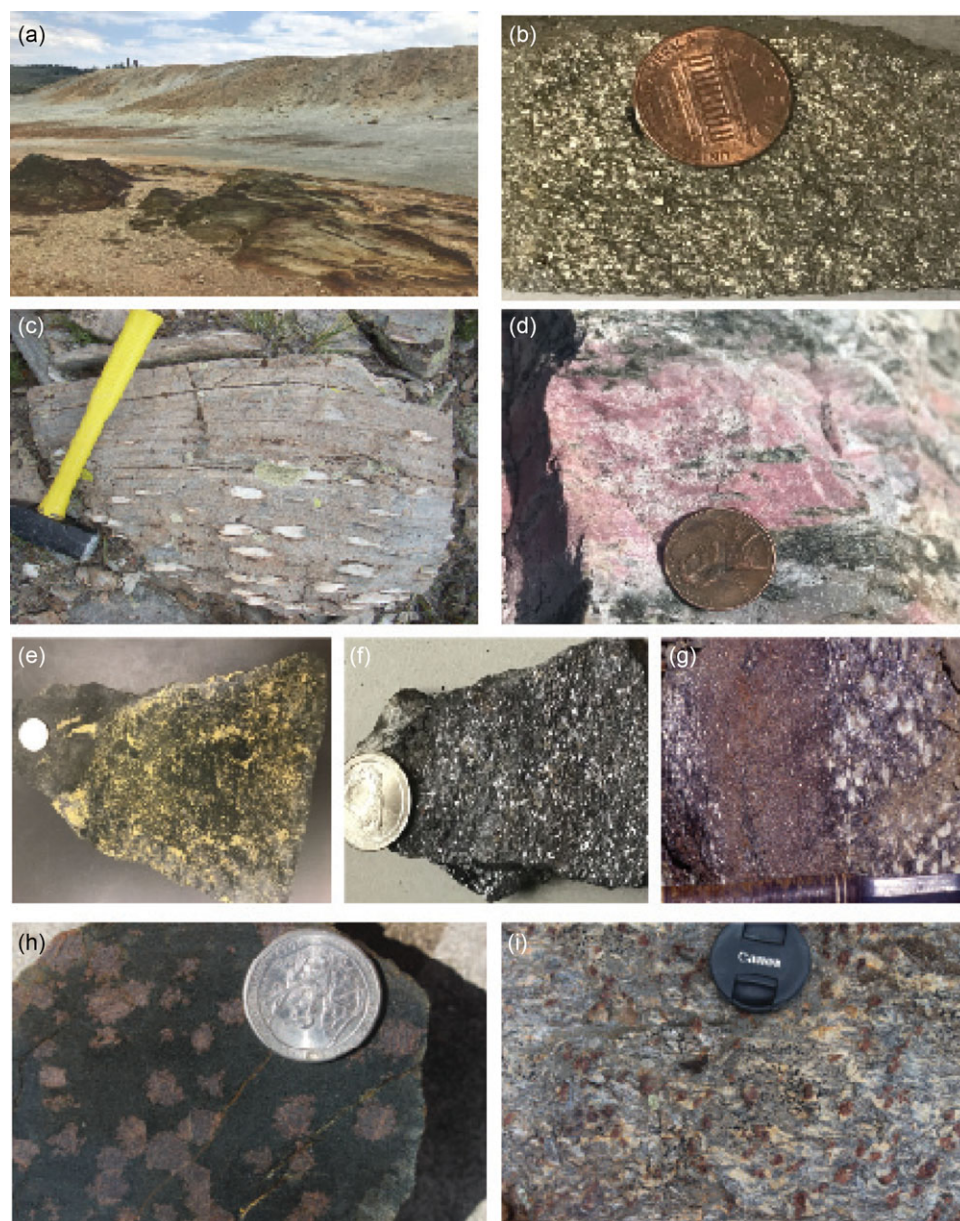


Figure 4. (Colour online) Sulphide samples, host rocks, metamorphosed altered rocks associated with the Vulcan, Bon Ton-Cinderella, Cotopaxi and Green Mountain deposits. (a) View of the tailings pile surrounding the Vulcan deposit. In the foreground are outcrops of oxidized pyrite-bearing quartz-muscovite schists; (b) massive pyrite-pyrrhotite-sphalerite ore from the Vulcan deposit; (c) nodular sillimanite rock grading into quartz-feldspar-biotite gneiss spatially related to the Cinderella deposit; (d) rhodonite-actinolite-quartz alteration spatially related to nodular sillimanite rock surrounding the Cinderella deposit; (e) semi-massive chalcopyrite from the Cotopaxi deposit; (f) massive sphalerite from the Cotopaxi deposit; (g) anthophyllite-cordierite-biotite gahnite rock surrounded by nodular sillimanite rock (Cotopaxi deposit); (h) garnet amphibolite spatially associated with the Green Mountain deposit; and (i) quartz-garnet-plagioclase-biotite rock spatially associated with the Green Mountain deposit. Note that this rock resembles the so-called Potosi Gneiss (a metamorphosed rhyodacite) spatially associated with the supergiant Broken Hill Pb-Zn-Ag deposit, Australia (Stevens & Barrons, 2002).

Sillimanite-quartz-muscovite-microcline gneiss, nodular sillimanite rock (Fig. 4c), biotite-muscovite schist, garnet gneiss, calc-silicate rocks, quartz-biotite-epidote gneiss and amphibolites are spatially associated with the Cinderella prospect. Iron formation occurs near the top of the stratigraphic sequence (D.C. Knight, unpub. MSc thesis, Univ. Manitoba, 1981). J. Ray, B. Ahlers, N. Shriver, K. Hattie and J. Shallow (unpub. report to American Copper and Nickel Company, 1993) reported two mineralized zones Zn-Cu and Pb-Zn-(Cu), which contain variable proportions of sphalerite, galena, chalcopyrite and pyrite, spatially related to nodular sillimanite rock and discontinuous zones of anthophyllite-rich rock. The lithologies at Bon Ton are essentially the same as those at Cinderella with nodular sillimanite rock enveloping mineralization in both locations, where it is up to 400 m wide and extends intermittently for 8 km. It is one of the most, if not the most, extensive nodular sillimanite horizons in Colorado (Spry *et al.* 2022b). The ‘nodules’

are composed of quartz and sillimanite with rare microcline, garnet and/or gahnite. Also present at Bon Ton is the spatial association of iron formation and gahnite to the sulphide mineralization (Heimann *et al.* 2005).

Metamorphosed altered rocks at Bon Ton consist of almandine-biotite-cordierite-quartz-gahnite-sphalerite \pm chlorite \pm muscovite \pm pyrite \pm chalcopyrite \pm pyrrhotite \pm plagioclase (andesine) \pm sillimanite and gahnite-biotite or phlogopite-quartz-sphalerite-pyrite-chalcopyrite-covellite \pm chlorite, while those at Cinderella contain the following assemblages: actinolite-phlogopite-garnet (spessartine)-gahnite, gahnite-anthophyllite-cordierite-phlogopite-tremolite \pm clinohumite \pm serpentine \pm sphalerite \pm pyrite, gahnite-chlorite-anthophyllite-cordierite-phlogopite-sillimanite \pm pyrite, phlogopite-quartz-garnet-gahnite-chlorite \pm anorthite \pm sillimanite and garnet-phlogopite-gahnite-quartz \pm K-feldspar. In places, rhodonite-actinolite-quartz rocks occur at Cinderella (Fig. 4d).

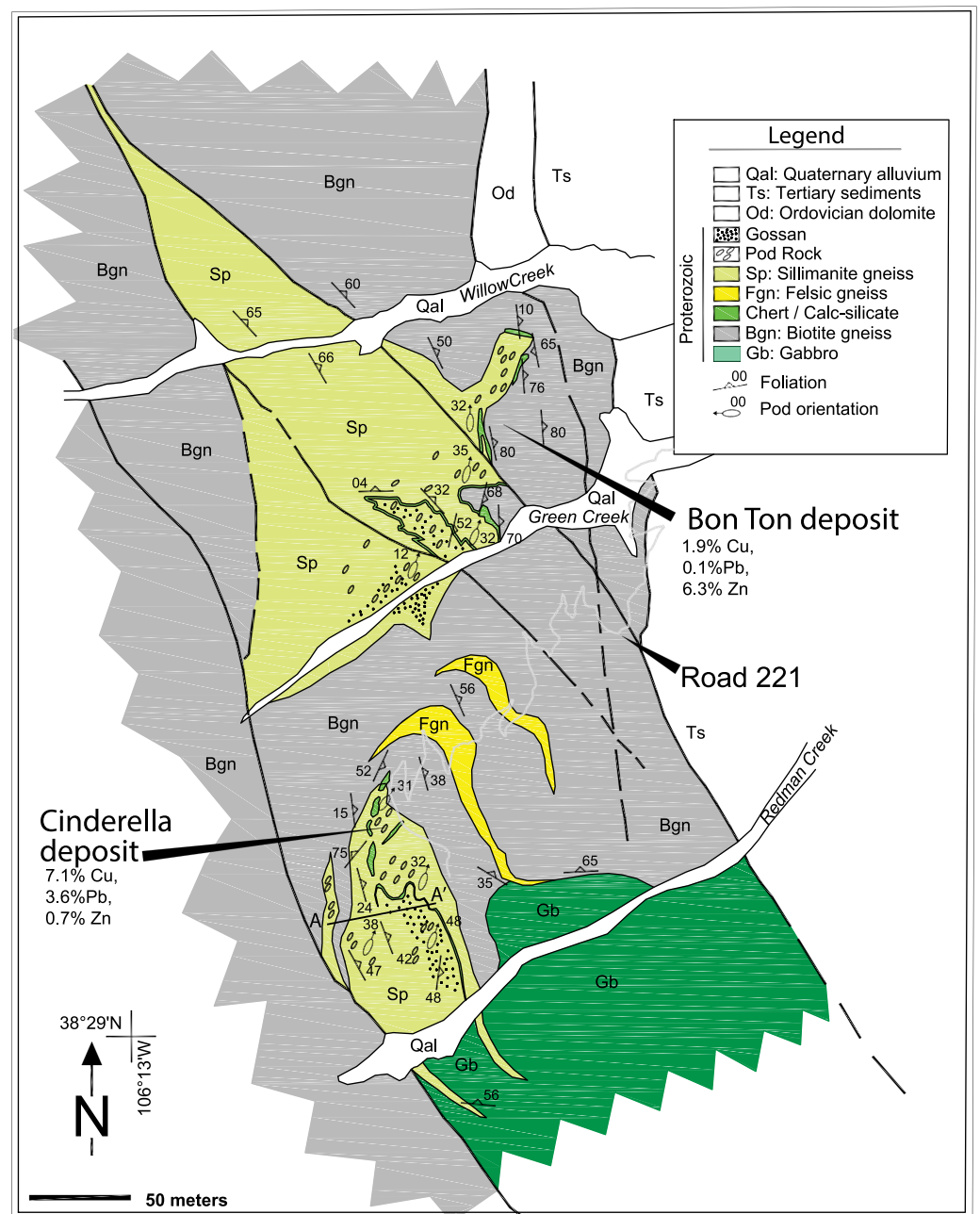


Figure 5. (Colour online) Geological map of the Cinderella-Bon Ton deposits showing the extensive intermittent nodular sillimanite rock horizon (~5 km long) that is spatially associated with sulphide mineralization in both deposits, which is hosted in biotite gneiss. Note the presence of metagabbro just to the south of the Cinderella deposit. The figure is modified after Spry *et al.* (2022b).

4.c. Cotopaxi

Cotopaxi is a well-studied Zn-Cu deposit located 1.6 km northwest of the town of Cotopaxi (e.g. Lindgren, 1908; Salotti, 1965). J. Ray, B. Ahlers, N. Shriver, K. Hattie and J. Shallow (unpub. report to American Copper and Nickel Company, 1993) noted that 1,316 t of Zn, 81 t of Cu, 70 t of Pb, 330 kg of Ag and 5 kg of Au were produced from the deposit since the 1880s. Biotite gneiss, quartz-feldspar biotite gneiss, hornblende gneiss, nodular sillimanite rock, amphibolite and pegmatitic rocks surround the sulphide mineralization in a package of rocks that is spatially associated with gneissic granite of the Boulder Creek batholith (Fig. 6). Salotti (1965) and Heinrich (1981) argued that the granitic gneiss constitutes a xenolith (1.2 km by 0.8 km) that formed as a roof pendant to the Boulder Creek gneissic granite. However, whether it is a xenolith remains uncertain due to the absence of clear contacts

between the metasedimentary package and the granite. Porphyroblasts of gahnite up to 3 cm in diameter occur in a variety of rock types (Heimann *et al.* 2005). Although cut by Proterozoic and Laramide faults, there is little evidence of local folding despite the presence of a dominant schistosity in the metasedimentary rocks. The main metallic minerals consist of pyrite, pyrrhotite, chalcocopyrite (Fig. 4e), sphalerite (Fig. 4f), gahnite and magnetite with minor amounts of molybdenite.

At Cotopaxi, a variety of metamorphosed altered rocks and ore-bearing assemblages are associated with sulphides, including anthophyllite-phlogopite-cordierite-gahnite ± rutile, actinolite-forsterite-gahnite-chalcocopyrite-galena-sphalerite ± pyrrhotite ± pyrite ± phlogopite ± magnetite ± clinohumite ± ilmenite ± covellite ± molybdenite, quartz-phlogopite-gahnite-sphalerite-galena-magnetite-rutile ± chalcocopyrite ± pyrrhotite ± molybdenite, cummingtonite-quartz-biotite-muscovite ± diopside ± olivine ± gahnite ±

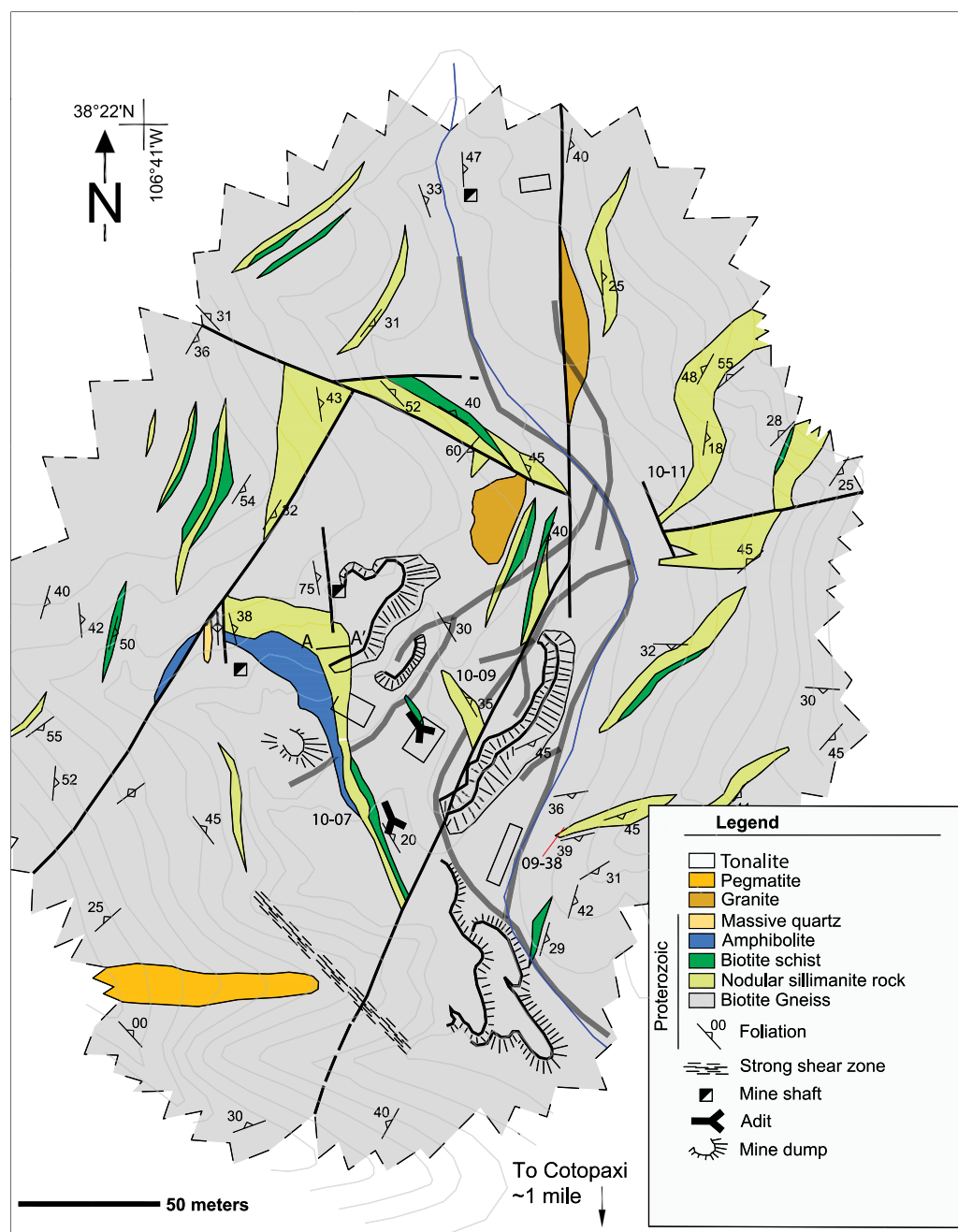


Figure 6. (Colour online) Geological map of the Cotopaxi deposit showing that the deposit is hosted in metasedimentary rocks and spatially associated with nodular sillimanite rocks and ‘amphibolite’ (anthophyllite-cordierite-biotite-gahnite altered rocks). The figure is modified after Salotti (1965) and Spry *et al.* (2022b).

clinohumite ± rutile ± sillimanite ± garnet ± plagioclase, K-feldspar ± zircon ± chalcopyrite ± galena ± sphalerite ± pyrite ± pyrrotite ± molybdenite ± magnetite ± ilmenite and hornblende-quartz-biotite-ilmenite ± garnet ± plagioclase ± cordierite ± gahnite ± epidote ± chalcopyrite ± sphalerite. These altered rocks locally occur in contact with nodular sillimanite rock (Fig. 4g).

4.d. Dawson-Green Mountain trend

4.d.1. Green Mountain

The Green Mountain Cu-Zn deposit, located in the Wet Mountains approximately 20 km southwest of Cañon City, occurs in migmatitic, quartz-feldspar-biotite and quartz-cordierite-biotite gneisses. Granodiorite of the Boulder Creek intrusion crops out 1.6 km northeast of the mine. G.T. Ririe (unpub. PhD thesis, Univ

Iowa, 1981) reported P-T conditions of 550° to 680°C and 4 kbar for rocks near the Green Mountain mine based on the stability of quartz, K-feldspar, Ca-rich plagioclase, hornblende, and minor sillimanite, biotite, almandine, and muscovite. Assuming a pressure of 4 kb, garnet-biotite geothermometry applied by A. Heimann (unpub. MS thesis, Iowa State Univ., 2002) to samples of garnet-biotite schist yields a temperature range of 510–628°C, which overlaps the temperature range estimated by G.T. Ririe (unpub. PhD thesis, Univ. Iowa, 1981).

Although the reserves of the deposit are unknown, a drilling programme by Phelps Dodge between 1979 and 1994 intersected two sulphide horizons; an upper zone of 2.3% Cu and 0.2% Zn over 1.2 to 3.3 m, and a lower zone of 18.1% Cu and 4.3% Zn over 1.5 m, which parallels sedimentary layering and a strong foliation identified by J. Ray, B. Alers, N. Shriver, K. Hattie and

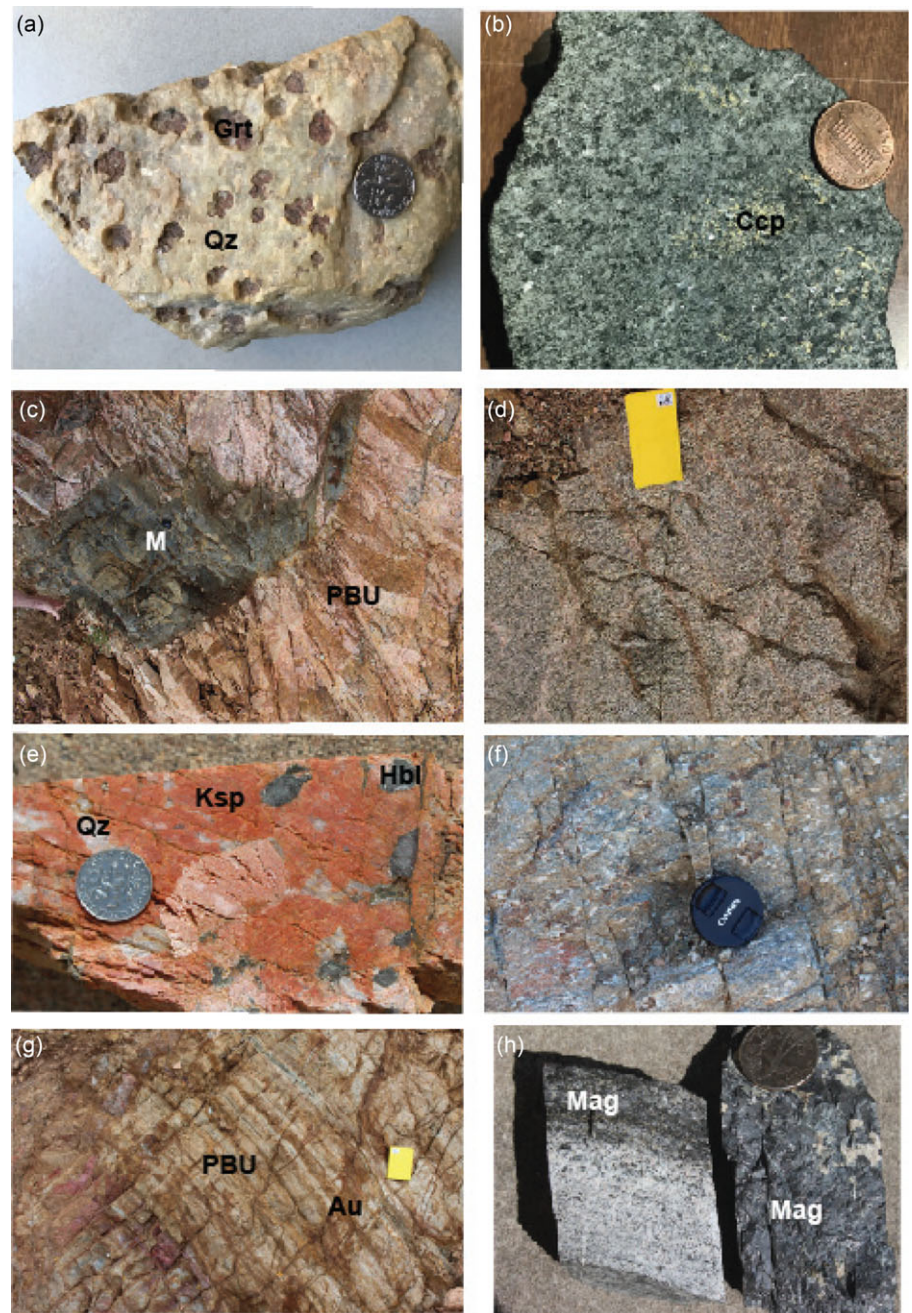


Figure 7. (Colour online) Rock samples from the Green Mountain and Dawson deposits. (a) Quartz (Qz)-garnet (Grt) exhalative/inhalative rock spatially associated with the Green Mountain deposit; (b) metamphibolite containing sphalerite and chalcopyrite (Ccp) from the Green Mountain deposit; (c) block of metasedimentary rock (M) in footwall pink granite (PBU) adjacent to the Dawson deposit. (d) monzodiorite from the hanging wall of the Dawson deposit; (e) coarse-grained alkali granite/pegmatite spatially associated with the Dawson deposit. Minerals are quartz (Qz), K-feldspar (Ksp) and hornblende (Hbl); (f) Quartz-garnet-plagioclase-biotite rock spatially associated with the Dawson deposit. Note this rock resembles that associated with the Green Mountain deposit (see Fig. 4i); (g) Pink banded unit (PBU) with late-stage cross-cutting gold-bearing veins (up to 92 g/t); (h) Banded quartz magnetite (Mag) rock (possible exhalative/inhalative rock) (left) and massive magnetite (right) in core from the Dawson deposit.

J. Shallow (unpub. report to American Copper and Nickel Company, 1993). Host rocks to ore are composed of nodular sillimanite-garnet±cordierite rock, quartz-garnet gneiss, anthophyllite-cordierite-gahnite rock, garnet amphibolite (Fig. 4h), garnet-sillimanite-feldspar gneiss (Fig. 4i), quartz-garnet rock (Fig. 7a), hornblende-quartz-biotite gneiss, quartz-biotite gneiss, garnet-bearing pegmatite, iron formation, biotite gneisses and minor calc-silicate gneiss. The garnet amphibolite is composed of garnet, hornblende, quartz, plagioclase and ilmenite. Metallic minerals consist of pyrite, pyrrhotite, sphalerite, chalcopyrite, gahnite and magnetite, with gangue minerals being dominated by biotite, anthophyllite, cummingtonite and clinopyroxene. Sulphides are generally disseminated in metamorphosed altered rocks consisting of anthophyllite-cummingtonite-gahnite-garnet ± pigeonite ± hornblende, as well as in gabbroic rocks (Fig. 7b).

4.d.2. Grape Creek trend

At least 30 minor prospects occur in the vicinity of Grape Creek in a linear trend that is the western extension of the Dawson area. The sheared package of metasedimentary rocks (up to ~120 m wide), consists mainly of quartz-K-feldspar-biotite±cordierite ±sillimanite±garnet rocks sandwiched between pink banded granite, which contains amphibolite sills, and biotite-quartz monzodiorite. The two largest prospects, west of Dawson, are Horseshoe and El Plomo, both of which contain massive sulphides in anthophyllite-rich altered rocks. The massive sulphides consist of pyrite, pyrrhotite, chalcopyrite, sphalerite, magnetite and gahnite, with galena present at El Plomo. The presence of this galena reflects a metallic zonation along the Grape Creek trend with more Cu-Zn mineralization to the east and Pb-Zn-Cu to the west. Although galena is a common repository of Ag in ore deposits

Table 2. Compositions of selected sulphides and sulphosalts

SAMPLE	TVD19-41	TVD19-31	TVD19-31	TVD-43	TVD-43
Deposit	El Plomo	El Plomo	El Plomo	Dawson	Dawson
Mineral	Tetrahedrite	Ag-tetrahedrite*	Ag-tetrahedrite*	Galena	Chalcopyrite
Cu wt%	33.74	12.85	13.75	0.01	33.12
Fe	2.72	5.53	3.56	0.02	30.53
Ag	3.84	33.94	32.08	0.31	0.17
Zn	3.82	0.29	2.61	0.01	0.01
Cd	1.57	0.19	0.48	0.06	0.01
Mn	0.01	0.00	0.01	0.01	0.00
Pb	0.04	0.03	0.06	85.00	0.09
As	0.00	0.00	0.00	0.00	0.00
Sb	29.49	26.23	26.21	0.00	0.00
Bi	0.02	0.02	0.00	0.44	0.07
S	24.70	20.31	20.63	13.52	34.98
Total	99.95	99.40	99.39	99.38	98.98
Cu at%	31.25	13.75	14.62	0.01	24.14
Fe	2.87	6.73	4.31	0.05	25.28
Ag	2.09	21.40	20.09	0.35	0.07
Zn	3.44	0.31	2.70	0.02	0.01
Cd	0.82	0.11	0.29	0.07	0.01
Mn	0.01	0.00	0.01	0.03	0.00
Pb	0.01	0.01	0.02	48.92	0.02
As	0.00	0.00	0.00	0.00	0.00
Sb	14.26	14.65	14.54	0.00	0.00
Bi	0.01	0.01	0.00	0.25	0.00
S	45.33	43.09	43.47	50.28	50.45

*Argentotetrahedrite.

(e.g. Both & Stumpfl, 1987), galena from El Plomo only contains up to 0.17 wt.% Ag and 0.41 wt.% Bi. Instead, Ag at El Plomo is contained in tetrahedrite (up to 4 wt.% Ag) and the rare mineral argentotetrahedrite, which contains up to 34 wt.% Ag (Table 2).

4.d.3. Dawson

The Dawson deposit occurs at the eastern end of the DGMT, where massive sulphides and gold mineralization are hosted in a narrow package of metasedimentary rocks (up to 50 m wide) adjacent to various granitoids (Fig. 8). A resource of ~4,250 kg Au was identified at a grade of 5 g/t Au (Zephyr Minerals, <https://www.zephyrminerals.com/dawson-section>). The metasedimentary package, which extends intermittently for over 5 km between Dawson and the eastern end of the Grape Creek segment, is sheared and faulted and consists of quartz-biotite-garnet (almandine) gneiss and quartz-biotite-muscovite-garnet±sillimanite ±cordierite±K-feldspar schists. The metasedimentary rocks also contain minor amounts of sulphides (pyrite, chalcopyrite, pyrrhotite and rare galena), gahnite, apatite and magnetite, with rare native gold (K. Wilson, unpub. report to U.S. Borax Ltd., 1982). To the north of the metasedimentary package is a pink banded gneiss (Fig. 7c) (herein referred to as the pink banded unit),

which is composed of pink-orange K-feldspar, quartz, and biotite with trace magnetite, pyrite, and hematite. It has a gradational contact with the metasedimentary package. Biotite-quartz monzonite/diorite (Fig. 7d) occurs on the southern side of the metasedimentary rocks and locally crosscuts it and the pink banded gneiss. The biotite-quartz monzonite/diorite is medium to coarse-grained and contains minor to trace amounts of magnetite, K-feldspar, serpentine, epidote, pyrite, chalcopyrite, amphibole and magnetite. Locally, this rock occurs as inclusions in biotite-K-feldspar gneiss.

Both granitoids (pink banded gneiss and biotite-quartz monzonite/diorite) are considered to have formed during the Yavapai orogeny based on granitoid ages, fabrics and mineralogical similarities elsewhere in the northern Wet Mountains (e.g. Siddoway *et al.* 2000). However, the age of the granitoids spatially associated with Dawson deposit is unknown due to the absence of geochronological studies. Other granitoids include an alkali granite (Fig. 7e) consisting of quartz, K-feldspar, biotite, and lesser amounts of magnetite and plagioclase just east of Dawson at Windy Point in addition to a volumetrically insignificant white coloured leucogranite. Enclaves of metasedimentary rocks occur in the pink banded unit suggesting that the

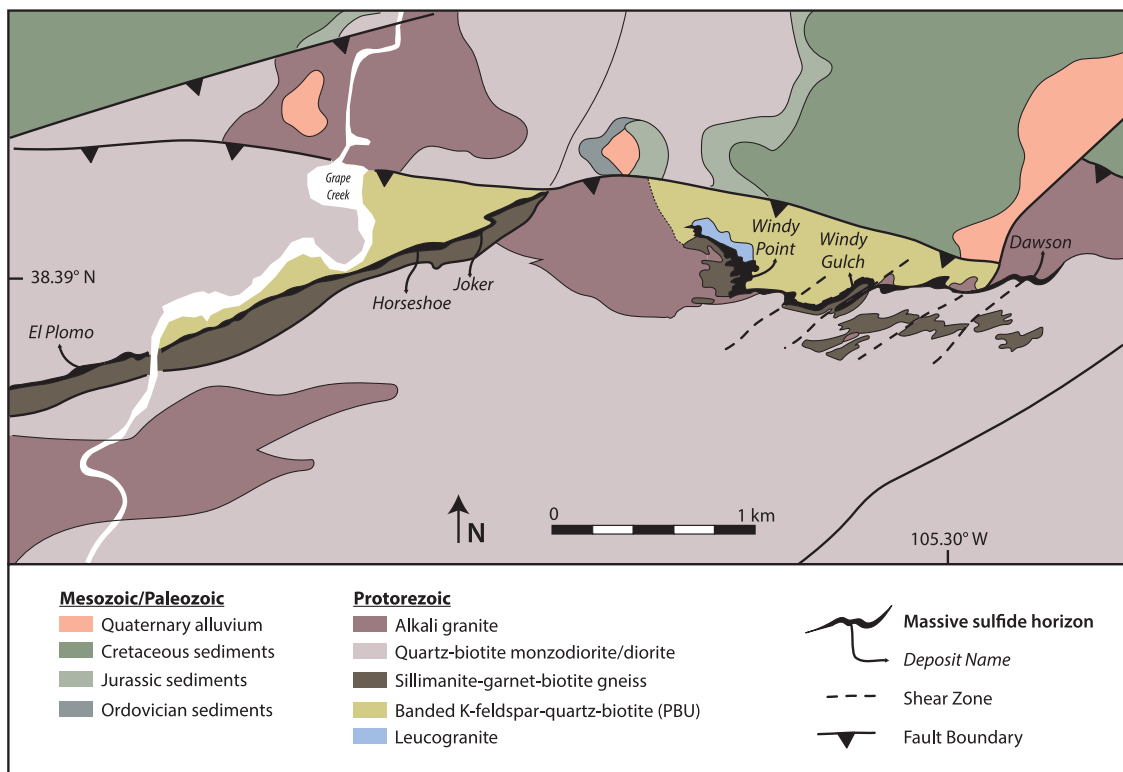


Figure 8. (Colour online) Geological map of the Dawson-Grape Creek trend. The Dawson area is subdivided into the Windy Point, Windy Gulch and Dawson segments. The so-called Grape Creek trend contains at least 30 minor prospects, the largest of which are Horseshoe and El Plomo. Note that the mineralized occurrences all occur in a narrow horizon of metamorphosed altered metasedimentary rocks between various granitoids. Part of the mineralized zone and host metasedimentary rocks were sheared and faulted.

metasedimentary rocks are older than the granitoid (Fig. 7c). Within the metasedimentary package are localized occurrences of quartz-garnet-sillimanite-feldspar gneiss (Fig. 7f) that resembles a rock spatially associated with the Green Mountain prospect (Fig. 4i). The mineralized zone is sheared and banded (Fig. 7g) and locally contains laminated iron formation and massive magnetite (Fig. 7h).

Mafic rocks include amphibolite, metagabbro and andesite dikes. Although uncommon, amphibolite dikes locally cross-cut quartz-garnet-biotite gneiss, while andesite dikes (up to 10 m wide) cut most rocks in the Dawson area. Small outcrops of metagabbro are present and has been intersected in drill core as sill-like bodies, where it contains inclusions of various gneisses (K. Wilson, unpub. report to U.S. Borax Ltd., 1982). It contains varying proportions of biotite, hornblende, plagioclase and chlorite, with trace amounts of pyrite, pyrrhotite and chalcopyrite.

The rocks were folded during three deformation episodes. The first fold event (F1) consists of isoclinal folds that shows a strong penetrative fabric, while F2 folds consist of tight asymmetrical folds that plunge in a S-SW direction. The third fold (F3) event consists of large regional scale horizontal folds.

There are three styles of mineralization at Dawson: polymetallic massive sulphide mineralization, disseminated gold mineralization and a late-stage gold overprint. Massive sulphide mineralization varies in width from a few centimetres to up to ~ 6 m wide and consists of, in order of abundance, pyrite, pyrrhotite, chalcopyrite and sphalerite with trace amounts of galena and marcasite in a horizon within the metasedimentary rocks. The sulphides vary from disseminated to massive (up to 50% sulphides) (Fig. 9a)

within a fragmented amphibole-chlorite-biotite-talc/serpentine-quartz rock. In places, the ore is brecciated and exhibits durchbewegt textures indicating sulphides were present prior to shearing (Fig. 9b). Brecciated fragments can be several centimetres in size with sulphides locally giving the appearance of having flowed around fragments. It is enclosed in a pervasive metamorphosed altered rock that consists of biotite-garnet-anthophyllite-cordierite±gahnite±hornblende± tremolite±magnetite.

Gold mineralization occurs in a strongly sheared siliceous garnet-biotite±sillimanite gneiss generally 6 to 7 m stratigraphically below the massive sulphide horizon (assuming stratigraphy is not overturned). However, in places, it occurs in contact with the massive sulphide unit. The gold-bearing unit contains disseminated pyrite and native gold occurs as isolated grains (Fig. 9c) or native gold occurs in silicates with other minor sulphides and Bi sulphosalts.

In the late-stage gold mineralization, E. von Pechmann (unpub. report to Uranerzbergbau GMBH, 1990) reported native gold in thin veinlets of quartz and siderite as well as isolated grains in cracks in garnet, sillimanite, biotite, anthophyllite, and sericite, along with pyrite, chalcopyrite, marcasite, and galena. He also reported the strong association between Au and Bi with the following Bi minerals being identified: hammarite ($\text{Bi}_4\text{Cu}_2\text{Pb}_2\text{S}_9$), friedrichite ($\text{Cu}_5\text{Pb}_5\text{Bi}_7\text{S}_{18}$), joseite-B ($\text{Bi}_4\text{Te}_2\text{S}$), krupkaite (AgBiSe_2) and possibly bohdanowiczite (AgBiSe_2). Petrographic and SEM studies here have also identified bismuthinite (Bi_2S_3) and unnamed phases in the system Bi-Se-S spatially associated with native gold (Fig. 9d). Galena from Dawson contains up to 0.35 wt.% Ag and 0.44 wt.% Bi (Table 2).

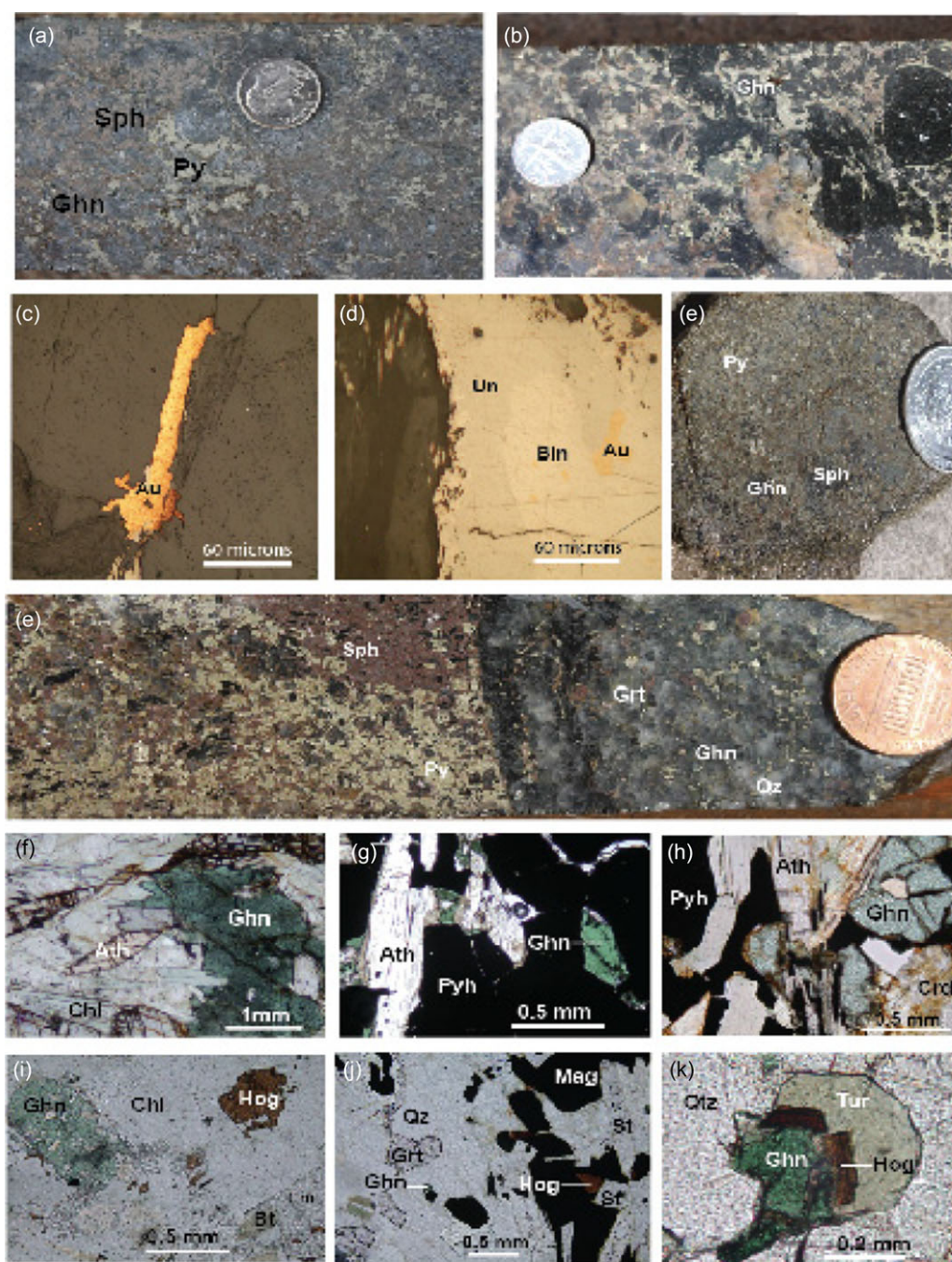


Figure 9. (Colour online) Ore samples and thin section micrographs of gahnite, anthophyllite/gedrite and högbomite-bearing rocks. (a) Massive sulphides containing pyrite (Py), sphalerite (Sph) and gahnite (Ghn) from the Dawson deposit. (b) Coarse gahnite in brecciated pyrite-bearing ore (Dawson deposit). (c) Veinlet of native gold (Au) in fracture in quartz (Qz) (Dawson deposit), reflected plain-polarized light. (d) Native gold (Au) along the contact between bismuthinite (Bin) and an unnamed Bi-Se-S phase (Un), reflected plain-polarized light. (e) Massive sulphides from the Horseshoe prospect consisting of pyrite (Py), sphalerite (Sph) and minor gahnite (Ghn). (f) Drill core showing massive sphalerite (Sp), pyrite (Py) on the left-hand side with quartz (Qz), pyrite (Py), gahnite (Ghn) and garnet (Grt) on the right-hand side. (g) Gahnite-anthophyllite (Ath)-chlorite (Chl) alteration spatially associated with sulphides from the Sedalia deposit. (h) Gahnite in pyrrhotite (Pyh) and in contact with anthophyllite in semi-massive ore (Green Mountain deposit). (i) Gahnite in contact with anthophyllite, pyrrhotite (Pyh) and cordierite (Crd) in disseminated sulphides (Dawson deposit), (plane-polarized light). (j) Högbomite (Hög) in gahnite-chlorite-corundum rock from the Independence deposit (plane-polarized light). (k) Högbomite in magnetite in contact with anthophyllite. Gahnite (Ghn), quartz (Qz) and garnet (Grt) occur in chlorite, plane-polarized light (Dawson deposit). (l) Inclusions of högbomite in contact with gahnite and tourmaline (Tur), plane-polarized light (Dawson deposit).

5. Results

5.a. Mineral compositions of altered rocks and sulphide zones

In a study of gahnite-bearing rocks spatially associated with massive sulphide deposits in Colorado, Heimann *et al.* (2005, 2006) obtained over 1500 electron microprobe analyses of oxides (gahnite, ilmenite and corundum) along with various silicates (i.e. biotite, amphibole, humite group minerals, garnet, cordierite, staurolite, plagioclase, chlorite, högbomite and pyroxene). Here, we focus on biotite, amphibole, garnet and gahnite, all of which are common in the metamorphosed altered rocks spatially associated with sulphides or as gangue minerals in massive sulphides in the DGMT, along with rare högbomite.

5.a.1. Amphiboles

Orthoamphiboles (gedrite and anthophyllite) and calcic amphiboles (magnesiornblende, actinolite, tremolite and tschermakite) are common in metamorphosed altered rocks spatially associated with mineralization in the DGMT, where gedrite and anthophyllite with blades that can exceed 1 cm in length are particularly common (Fig. 9i, j). Orthoamphiboles from the Dawson, Green Mountain, El Plomo and Horseshoe deposits consist of anthophyllite and gedrite with Mg/(Mg+Fe) ratios generally ranging between 0.6 and 0.8 (Fig. 10a). These minerals are intergrown with biotite, cordierite, gahnite and disseminated metallic minerals (pyrite, pyrrhotite, chalcopyrite, sphalerite, magnetite and rare galena). Calcic amphiboles occur in the same four locations as the orthoamphiboles, as well as the small Joker prospect, just east of the

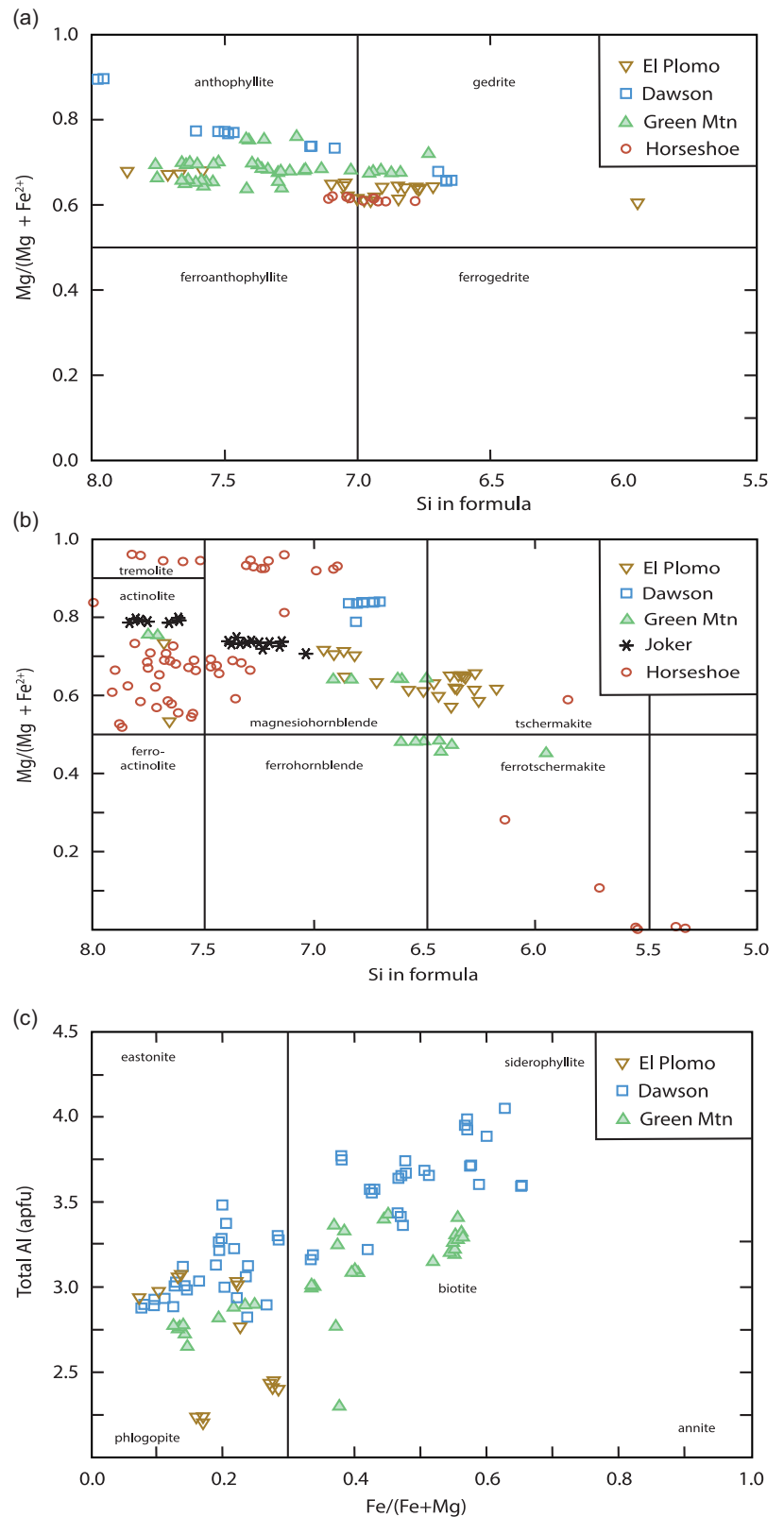


Figure 10. (Colour online) Binary plots of amphibole and biotite compositions from the Dawson-Green Mountain trend as a function of Mg/(Mg+Fe) vs Si. (a) Orthorhombic Mg-Fe-Mn amphiboles ((Ca+Na) <1.00; (Mg, Fe²⁺, Mn) ≥ 1.00). (b) Calcic amphiboles (Ca ≥ 1.50; (Na+K) <0.05). (c) Biotite compositions as a function of total Al vs Fe/(Fe+Mg).

Horseshoe prospect. They commonly coexist with orthoamphiboles in the same rock but are generally less abundant and are finer grained. The calcic amphiboles show a broad range of compositions and include tremolite, actinolite, magnesiohornblende and

tschermakite with Mg/(Mg+Fe) ratios ranging from 0.52 to 0.97 (Fig. 10b). Analyses of amphiboles from a garnet amphibolite from the Green Mountain deposit has a lower Mg content with Mg/(Mg+Fe) ratios ranging from 0.46 to 0.48 (Table 3).

Table 3. Representative compositions of amphibole and biotite

Mineral	Bt	Bt	Bt	Bt	Ath	Hbl	Ged	Ath	Hbl	Ged
Deposit	GM	GM	Dawson	Dawson	Horseshoe	Horseshoe	Dawson	GM	Dawson	Dawson
Sample	TVD19-91	TVD19-93	TVD19-22	TVD19-25	TVD19-60	TVD19-60	TVD-30	TV19-92	TVD-76	TVD-53
Analyses (n)	9	2	4	5	5	4	6	32	8	4
SiO ₂ wt. %	38.25	35.45	41.19	38.67	47.98	42.93	44.28	50.96	44.38	48.03
TiO ₂	0.51	1.69	0.30	0.38	0.19	0.75	0.17	0.18	0.48	0.14
Al ₂ O ₃	16.27	19.07	12.41	13.48	8.62	13.19	15.03	5.04	12.37	10.56
FeO	7.51	18.01	8.21	12.89	20.43	14.46	17.09	17.45	6.88	13.79
MnO	0.01	0.02	0.22	0.59	0.56	0.23	0.33	0.66	0.27	0.74
MgO	22.83	12.44	23.15	18.93	18.25	13.10	18.35	21.68	18.28	21.65
CaO	0.02	0.01	0.01	0.01	0.61	10.36	0.58	0.73	10.95	0.38
Na ₂ O	0.69	0.25	0.65	0.06	1.04	1.63	1.70	0.68	1.70	1.24
K ₂ O	8.77	9.31	9.30	9.99	0.00	0.25	0.00	0.09	0.22	0.01
ZnO	0.00	0.09	0.15	0.09			0.07		0.05	0.13
F	1.00	0.32	2.86	2.09						
Cl	0.02	0.05	0.04	0.07			0.01		0.01	0.01
Total	95.88	96.71	98.49	97.25	97.68	96.9	97.61	97.47	95.59	96.68
Cations per 22 oxygens for biotite and 23 oxygens for amphiboles										
Si	5.526	5.385	6.275	5.928	6.706	6.031	6.381	6.997	6.453	6.857
Ti	0.055	0.193	0.035	0.044	0.02	0.079	0.018	0.018	0.052	0.015
Al	2.77	3.413	2.229	2.435	1.36	2.183	2.552	0.817	2.122	1.788
Fe	0.906	2.288	1.046	1.652	2.388	1.559	2.059	2.004	0.843	1.647
Mn	0.002	0.002	0.028	0.077	0.066	0.027	0.04	0.077	0.033	0.089
Mg	4.917	2.818	5.257	4.326	3.803	2.744	3.941	4.438	3.959	4.609
Ca	0.003	0.001	0.002	0.002	0.091	1.559	0.089	0.108	1.705	0.058
Na	0.193	0.074	0.191	0.017	0.283	0.445	0.475	0.181	0.479	0.342
K	1.616	1.803	1.808	1.955	0.001	0.047	0.001	0.016	0.041	0.001
Zn	0	0.01	0.017	0.01			0.007		0.006	0.013
F	0.459	0.155	1.381	1.015						
Cl	0.005	0.012	0.01	0.019			0.001		0.004	0.002

Ath, anthophyllite; Bt, biotite; GM, Green Mountain; Ged, gedrite; Hbl, hornblende.

5.a.2. Biotite

Biotite in metamorphosed altered rocks from the Dawson, Green Mountain and El Plomo deposits range from phlogopite to siderophyllite with Fe/(Fe+Mg) and total Al (apfu) ratios varying from 0.06 to 0.65 and 2.0 to 4.1, respectively (Fig. 10c). Biotite from the El Plomo deposit plots entirely within the phlogopite field. Halogen (F and Cl) concentrations of biotite show elevated concentrations of F in samples TVD19-22 and TVD19-25 from El Plomo that contain up to 3.24 and 2.13 wt% F, respectively, with up to 1.2 wt% F and 1.3 wt% F also occurring in biotite from the Green Mountain (TVD19-89), and Dawson (TVD-43) deposits, respectively (Table 3). It should be noted that biotite in samples with the lowest Fe/(Fe+Mg) ratios have the highest concentrations of F, which is consistent with Fe-F avoidance in F-bearing biotite reported previously by, for example, Valley *et al.* (1982), Zaleski *et al.* (1991) and Rosenberg *et al.* (2000).

5.a.3. Garnet

Garnet-bearing rocks from the Dawson area consist primarily of metamorphosed garnet-biotite-cordierite-gahnite altered rocks and in biotite-sillimanite-garnet schists while those from Green Mountain consist of garnet-bearing amphibolite (TVD19-79), quartz-biotite-garnet-gahnite rock (TVD19-84), and massive (TVD19-85) or laminated (TVD19-81, TVD19-93) garnet-quartz±biotite rocks (Fig. 7a, b). The massive and laminated garnet-bearing rocks resemble quartz garnetites spatially associated with metamorphosed Sedex, BHT and VMS deposits elsewhere (e.g. Spry *et al.* 2000). Garnet from the metamorphosed altered rocks associated with the Dawson deposit are almandine-rich (shown as mole% end-member molecule) with lesser amounts of pyrope and minor amounts of the spessartine, grossular and andradite molecules (Alm₇₄₋₈₂Prp₁₁₋₁₇Sps₂₋₈Grs₂₋₃Adr_{<1}, Fig. 11a, Table 4). These compositions are similar to those

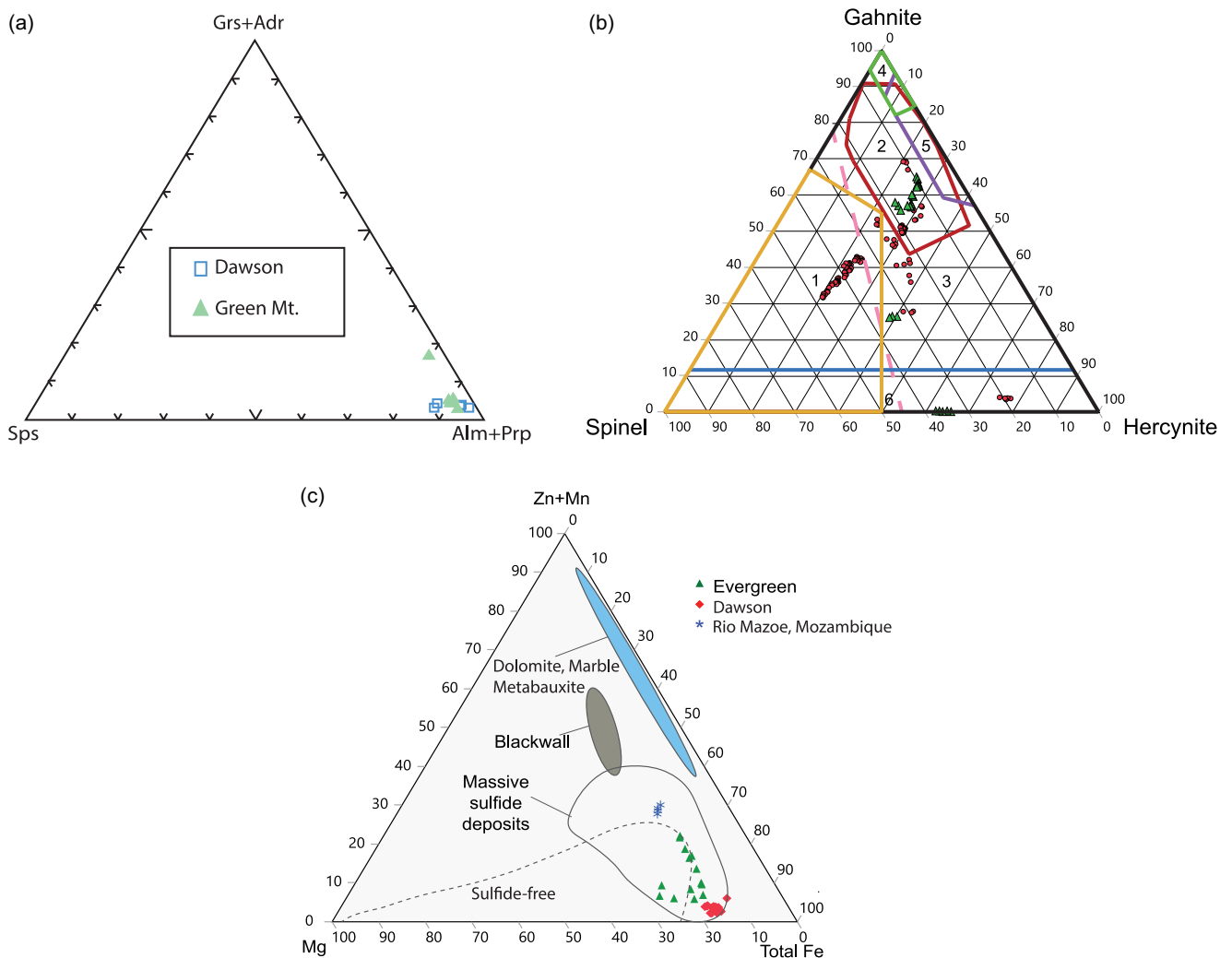


Figure 11. (Colour online) Ternary plots of (a) Garnet, (b) Zincian spinels and (c) Högbomite from the Dawson-Green Mountain trend. Garnet is plot in terms of spessartine, grossular + andradite and almandine + pyrope. The zincian spinels are plot terms of the gahnite-hercynite-spinel *sensu stricto* spinel end-members from the Dawson, Green Mountain and Horseshoe deposits. Numbers correspond to compositional ranges of gahnite from different geological settings as defined by Spry *et al.* (1986) and Heimann *et al.* (2005): 1. marbles, 2. metamorphosed massive sulphide deposits and S-poor rocks in Mg-Ca-Al alteration zones, 3. metamorphosed massive sulphide deposits in Fe-Al metasedimentary and metavolcanic rocks, 4. metabauxites, 5. pegmatites, 6. unaltered and hydrothermally altered Fe-Al rich metasedimentary and metavolcanic rocks, and 7. Al-rich granulites. The högbomite compositions are shown for aluminous metasediments, ultramafic rocks, calcic skarns, Fe-Ti deposits and calc-silicate granulites reported by Spry & Petersen (1989), quartzofeldspathic gneisses (Grew *et al.* 1990), metabauxites (Yalçin *et al.* 1993; Feenstra 1997; Ockenga *et al.* 1998), cordierite gneisses (Heimann *et al.* 2006), pelites (Rakotonandrasana *et al.* 2010) dolomitic marble (Armbruster *et al.* 1998) and blackwall (Owens *et al.* 2013).

previously obtained by K. Wilson (unpub. report to U.S. Borax Company, 1982) from Dawson and by Sheridan and Raymond (1984b) from the Sedalia deposit who reported garnet with a composition of 78 mole% almandine, 10 mole% pyrope, and smaller quantities of the spessartine and grossular molecules. Garnet from the Dawson deposit is more enriched in the almandine molecule and less enriched in pyrope than garnet in the various garnet-bearing rock types from Green Mountain ($\text{Alm}_{67-75}\text{Prp}_{16-24}\text{Sps}_{3-5}\text{Grs}_{3-4}\text{Adr}_{<2}$). A single sample of garnet-bearing amphibolite from the latter deposit is more enriched in the grossular end-member than all the other garnets analysed here ($\text{Alm}_{66}\text{Prp}_{15}\text{Sps}_3\text{Grs}_{15}\text{Adr}_{<2}$).

5.a.4. Gahnite

Although some compositional data were obtained for gahnite from the Green Mountain deposit by Heimann *et al.* (2005), no gahnite compositions have previously been determined from the

Horseshoe, El Plomo and Dawson deposits. New compositions of gahnite in the metamorphosed altered rocks spatially associated with the DGMT deposits are discussed here. Table 5 shows the location, lithologies, mineralogy of the samples from which gahnite compositions were obtained, along with the average end-member spinel molecules (gahnite (Ghn), hercynite (Hc), spinel *sensu stricto* (Spl) and galaxite (Glx)). The compositions of representative gahnite compositions are given in Table 6, while all gahnite data obtained here are in Supplementary Appendix Table S1. Gahnite in sulphide-rich zones consist of approximately >10% visible sulphides (pyrite, pyrrhotite, chalcopyrite and sphalerite), whereas metamorphosed altered rocks in contact with sulphide zones generally contain <10% visible sulphides, with some containing no visible sulphides. In the sulphide zone at Dawson, drill hole DA18-16 (samples TVD-70 to TVD-76), sulphides are spatially associated with gahnite that predominantly occurs in contact with various silicates, including phlogopite, anthophyllite/

Table 4. Average major element compositions of garnet

Deposit	Dawson	Dawson	Dawson	Dawson	Dawson	Green Mt.	Green Mt.	Green Mt.	Green Mt.	Green Mt.	Green Mt.
Sample no.	TVD-3B	TVD-6	TVD-7	TVD-40B	TVD-50	TVD19-79	TVD19-81	TVD19-84	TVD19-85	TVD19-87	TVD19-93
n	6	2	3	6	12	4	4	12	16	4	3
SiO ₂	37.02	36.79	37.05	37.22	36.82	37.09	37.48	37.34	36.99	36.78	37.49
TiO ₂	0.01	0.00	0.01	0.00	0.01	0.01	0.00	0.01	0.00	0.01	0.00
Al ₂ O ₃	20.77	20.62	20.71	20.87	20.73	20.53	21.17	21.15	20.78	20.41	21.26
FeO	37.44	37.07	34.16	35.88	36.87	31.11	31.50	30.87	33.67	34.47	33.38
MnO	1.66	1.63	4.24	0.07	3.60	1.50	1.83	2.23	2.31	1.94	1.40
MgO	2.98	2.97	3.41	4.43	2.77	3.47	5.92	6.19	4.14	3.95	5.24
CaO	0.07	0.75	0.61	0.80	1.22	5.37	1.58	1.17	1.32	1.04	1.12
Total	100.61	99.83	100.19	99.91	100.02	99.23	99.62	99.07	99.30	98.69	99.97
Number of atoms in formulae (oxygen basis 12)											
Si	2.990	2.990	2.992	2.989	2.986	2.982	2.973	2.973	2.983	2.993	2.979
Ti	0.000	0.000	0.001	0.000	0.001	0.001	0.000	0.000	0.000	0.000	0.000
Al	1.975	1.975	1.970	1.975	1.982	1.945	1.979	1.985	1.976	1.957	1.992
Fe ²⁺	2.502	2.495	2.277	2.385	2.347	2.036	2.069	2.041	2.247	2.303	2.211
Fe ³⁺	0.025	0.025	0.030	0.025	0.018	0.055	0.021	0.015	0.024	0.043	0.008
Mn	0.113	0.112	0.290	0.050	0.247	0.102	0.123	0.150	0.158	0.134	0.094
Mg	0.358	0.360	0.410	0.529	0.335	0.416	0.700	0.735	0.498	0.479	0.621
Ca	0.064	0.065	0.053	0.068	0.106	0.463	0.134	0.100	0.114	0.091	0.095
	3.062	3.057	3.060	3.057	3.053	3.072	3.048	3.041	3.040	3.049	3.029
Almandine	81.71	81.62	74.41	78.02	76.88	66.28	67.89	67.12	73.91	75.52	72.99
Andradite	0.82	0.82	0.98	0.82	0.59	1.79	0.69	0.49	0.79	1.41	0.26
Grossular	2.09	2.13	1.73	2.22	3.47	15.07	4.41	3.28	3.76	2.97	3.14
Pyrope	11.69	11.78	13.40	17.30	10.97	13.54	22.97	24.17	16.36	15.71	20.50
Spessartine	3.69	3.66	9.48	1.64	8.09	3.32	4.04	4.94	5.18	4.38	3.11

TVD-3B garnet-biotite rock; TVD-6 quartz-garnet-biotite altered rock; TVD-7; TVD-40B garnet-gahnite-biotite-anthophyllite altered rock; TVD-50 laminated biotite-quartz rock; TVD19-79 garnet amphibolite; TVD19-81 garnet-quartz-biotite rock; TVD19-84 quartz-garnet-gahnite rock; TVD19-85 garnet-biotite-quartz rock; TVD19-87 garnet-biotite-quartz rock; TVD19-93 garnet-biotite-quartz rock.

gedrite, cordierite and muscovite in the absence of quartz. In these samples, gahnite compositions are generally similar ($\text{Ghn}_{33-42}\text{Hc}_{20-24}\text{Spl}_{34-47}$, Fig. 11b). In sample TVD19-52 in drill hole GC2, a quartz-bearing sulphide specimen has the highest gahnite component of all samples analysed here ($\text{Ghn}_{71}\text{Hc}_{21}\text{Spl}_8\text{Gl}_1$). In contrast, gahnite in metamorphosed altered rocks from the Dawson deposit are considerably more variable and contain higher proportions of the gahnite and hercynite molecules and lower concentrations of the spinel end-member ($\text{Ghn}_{32-55}\text{Hc}_{23-40}\text{Spl}_{14-27}$). Two non-sulphide-bearing altered rocks from the Sentinel prospect (immediately west of the main Dawson mineralized zone) contain gahnite with extremely variable compositions ($\text{Ghn}_{4-68}\text{Hc}_{21-77}\text{Spl}_{10-20}$). Gahnite in a quartz-bearing sulphide-rich rock from the Green Mountain deposit has a similar composition ($\text{Ghn}_{69}\text{Hc}_{24}\text{Spl}_6\text{Gl}_1$) to that in drill hole GC2 from Dawson. Those in altered rocks that contain similar minerals to those associated with the Dawson deposit have the following compositions ($\text{Ghn}_{0.4-55}\text{Hc}_{27-67}\text{Spl}_{16-43}$), while those in coarse quartz-garnet rocks show a narrower range of compositions and a generally lower amount of the spinel end-member ($\text{Ghn}_{41-58}\text{Hc}_{32-45}\text{Spl}_{10-18}$).

5.a.5. Högbomite

Högbomite, and its zincian counterpart zincohögbomite, are complex Fe-Mg-Zn-Al-Ti oxides that are composed of spinel and nolanite molecules (Armbruster, 2002). They occur in various rock types metamorphosed to the upper amphibolite-granulite facies, including aluminous metasediments, ultramafic rocks Fe-Ti deposits, skarns, Fe ores and metamorphosed massive sulphide deposits (e.g. Teale, 1980; Spry & Petersen, 1989; Feenstra 1997; Rakotonandrasana *et al.* 2010; Owens *et al.* 2013). In Colorado, Gable and Sims (1969) reported högbomite in cordierite-bearing gneisses in the central Front Range, where it occurs along the contact between hercynite and magnetite or ilmenite. Ferrohögbomite (between 1.7 and 8.6 wt.% ZnO) was identified by Heimann *et al.* (2006) from the Evergreen prospect, where it occurs in a corona of cordierite, hercynite, corundum, staurolite, and sillimanite along the contact between ilmenite and magnetite within gedrite-cordierite-garnet gneiss, while Heinrich and Griffiths (1948) noted its presence in the Turret mining districts in a corundum-chlorite-spinel rock. We identified högbomite from the Independence deposit in this district where it occurs in samples

Table 5. Gahnite-bearing rocks and spinel sensu stricto end members from the Dawson, El Plomo, Green Mountain, and Horseshoe deposits

Deposit	Sample no.	Location	Lithology	Mineralogy of gahnite-bearing rock*	Ghn	Hc	Spl	Glx
Dawson	TVD-12	WG16-27 67.0	Altered rock	Phl, Ghn, Sp, Chl, Ccp, Zrn	40.79	34.00	24.28	0.93
Dawson	TVD-15	WG16-27 79.1	Altered rock	Tlc ² , Bt, Ath, Ghn, Py ¹ , Ccp ¹ , Sp ¹	32.73	39.66	26.94	0.67
Dawson	TVD-18	WG16-27 83.3	Altered rock	Crd, Tlc ² , Ath, Bt, Ghn, Py, Ccp, Sp	46.60	29.04	24.07	0.29
Dawson	TVD-39	Outcrop (Sentinel)	Altered rock	Bt, Ser, Pl, Ghn, Qz	68.19	21.08	10.16	0.57
Dawson	TVD-40B	Outcrop (Sentinel)	Altered rock	Bt, Ath, Ghn, Grt, Mag, Hbl, Py 1, Ccp 1, Tur 1, Hgb	3.92	76.52	19.56	0.00
Dawson	TVD-53	WG13-14 57.5	Altered rock	Ath, Ghn, Bt, Sp	52.28	22.88	24.65	0.19
Dawson	TVD-70	DA18-16 604.2	Sulphide zone	Phl, Py, Pyh, Ccp, Ghn, Ath, Crd, Chl	40.94	23.55	35.32	0.18
Dawson	TVD-71	DA18-16 605.5	Sulphide zone	Phl, Py, Ccp, Ccp, Ghn, Sp, Chl	38.21	22.37	39.14	0.28
Dawson	TVD-72	DA18-16 608.0	Sulphide zone	Phl, Ccp, Py, Pyh, Ghn, Crd, Sp	32.66	20.48	46.57	0.29
Dawson	TVD-73	DA18-16 610.0	Sulphide zone	Phl, Po, Pyh, Ghn, Ccp, Sp	35.71	21.65	42.36	0.28
Dawson	TVD-74	DA18-16 611.7	Sulphide zone	Phl, Po, Pyh, Ghn, Ms, Crd, Sp, Pl, Ccp, Chl, Mnz	42.38	23.01	34.32	0.29
Dawson	TVD-75	DA18-16 616.7	Sulphide zone	Bt, Py, Chl, Ghn, Ath, Pyh, Sp, Cal, Ccp	35.82	20.94	42.93	0.31
Dawson	TVD-76	DA18-16 618.7	Sulphide zone	Chl, Py, Pyh, Ms, Tlc, Ath, Ghn, Hbl, Ccp	41.12	22.12	36.47	0.29
Dawson	TVD-77	DA18-16 619.5	Altered rock	Qz, Crd, Ghn, Sil, Po, Ccp, Sp, Tur	54.75	30.66	14.11	0.48
Dawson	TVD-78	DA18-16 624.0	Altered rock	Qz, Crd, Po, Ccp, Ghn, Sp, Tur	50.33	29.38	19.91	0.38
Dawson	TVD19-13	WG13-12 74.0	Altered rock	Ath, Bt, Ghn	36.51	39.81	23.30	0.28
Dawson	TVD19-17	GC27 484	Mag rock	Bt, Cal, Pl, Grt, Qz, Mag, Hgb	20.12	16.61	62.78	0.49
Dawson	TVD19-52	GC2 181	Sulphide zone	Qz, Ghn, Po, Py, Bt, Ccp, Ms, Sp	71.00	20.86	7.48	0.66
Green Mt.	TVD19-80	Dump	Mag-Ath rock	Mag, Ath, Ghn	17.29	55.08	27.45	0.18
Green Mt.	TVD19-84	Dump	Qz-Grt rock	Qz, Crd, Bt, Ghn, Tur, Zrn	41.27	40.70	17.84	0.19
Green Mt.	TVD19-87	Dump	Grt-Bt rock	Qz, Bt, Grt, Ms, Ghn 1, Mnz	58.11	32.16	9.64	0.09
Green Mt.	TVD19-88	Dump	Altered rock	Grt, Qz, Bt, Ghn	40.75	27.35	31.70	0.20
Green Mt.	TVD19-89	Dump	Altered rock	Bt, Ghn, Mag, Ap, Mnz, Chl, Py, Ccp	3.77	67.41	28.28	0.54
Green Mt.	TVD19-91	Dump	Altered rock	Phl, Mag, Ghn, Ser, Crd?	0.37	55.66	43.62	0.35
Green Mt.	TVD19-92	Dump	Altered rock	Ath, Ghn, Mag	47.03	29.22	23.47	0.28
Green Mt.	TVD19-93	Dump	Qz-Grt rock	Qz, Grt, Bt, Ghn	42.61	45.11	12.19	0.09
Green Mt.	TVD19-96	Dump	Altered rock	Hbl, Ghn, Crd, Sp, Ccp, Phl	55.31	28.81	15.70	0.18
El Plomo	TVD19-37	Dump	Sulphide zone	Qz, Ghn, Pl, Py, Pyr, Ccp, Bt, Sp	69.30	23.91	5.67	1.12
Horseshoe	TVD19-66	Dump	Altered rock	Ath, Ghn, Qz, Pl, Crd, Ol?	36.10	47.39	15.86	0.65

*Mineral abbreviations after Warr (2021).

¹Trace amounts.

²Secondary mineral.

SAM09-51 and SAM09-53 (up to 0.5 mm in length) in the metamorphosed alteration zone of the deposit with chlorite, gahnite, corundum, biotite, magnetite and sericitized cordierite. The latter sample also contains coarse garnet. The composition of two ferrohögbomite-bearing samples from the Dawson district (samples TVD-40B and TVD19-17) is given in Table 6 and shown in Fig. 11c. In sample TVD19, ferrohögbomite occurs in contact with magnetite and biotite in strongly altered cordierite that was replaced by sericite and late calcite. The samples contain up to 2.3 and 5.3 wt.% ZnO, respectively. For comparative purposes, we include a previously unpublished composition of a zinc-bearing ferrohögbomite from the metamorphosed Rio Mazoe base metal district, Mozambique. It contains up to 10.0 wt.% ZnO and occurs along the contact between magnetite and zincian spinel, the latter of which contains between 21 and 23 wt.% ZnO (Table 6).

5.a.6. Sulphides

In an attempt to apply the sphalerite geobarometer of Hutchison and Scott (1981) to determine the peak pressures of metamorphism that affected the deposits, sphalerite in contact with pyrite and pyrrhotite was evaluated. However, application of the geobarometer was unsuccessful because pyrrhotite is primarily monoclinic rather than the required hexagonal form. Nevertheless, sphalerite in contact with both pyrite and pyrrhotite or pyrrhotite alone contains between 6.2 and 10.0 wt.% Zn, with more than 95% of values between 6.5 and 8.0 wt.% of Zn regardless of the metamorphic grade of the deposit. Sphalerite coexisting with pyrite only contains between 2.7 and 5.7 wt.% Zn, with one anomalous sample from Cotopaxi containing approximately 0.4 wt.% Zn. The Cd content of sphalerite using a count time of 60 seconds on the Cd peak is 1920 to 2680 ppm (Supplementary Appendix Table S2a),

Table 6. Representative average compositions of gahnite and högbomite

Mineral	Gahnite	Gahnite	Gahnite	Gahnite	Gahnite	Högbomite	Högbomite	Högbomite
Deposit	Dawson	Dawson	Dawson	Horseshoe	Green Mt	Dawson	Dawson	Rio Mazoe
Sample no	TVD-39	TVD-71	TVD19-17	TVD19-66	TVD19-96	TVD-40B	TVD19-17	1116
n	4	4	1	10	9	14	7	5
SiO ₂	0.01	0.00	0.06	0.01	0.01	0.10	0.05	0.01
TiO ₂	0.02	0.00	0.51	0.01	0.00	5.37	5.07	5.02
Al ₂ O ₃	54.88	59.47	56.62	59.72	55.16	61.52	57.88	57.52
FeO	8.97	10.31	26.58	7.42	12.64	28.60	25.32	19.56
MnO	0.25	0.12	1.03	0.32	0.09	0.09	1.00	1.83
MgO	2.43	10.13	3.94	12.43	3.86	3.23	3.75	3.04
ZnO	32.84	19.96	9.65	19.11	27.49	1.33	3.19	9.15
Total	99.40	100.00	99.84	99.65	99.63	100.25	96.26	96.36
Number of cations in formulae (gahnite 3; högbomite 22)								
Si	0.000	0.000	0.002	0.000	0.000	0.021	0.010	0.001
Ti	0.000	0.000	0.011	0.000	0.000	0.835	0.816	0.823
Al	1.938	1.934	1.938	1.928	1.917	14.982	14.608	14.770
Fe	0.222	0.239	0.646	0.170	0.312	4.942	4.684	3.566
Mn	0.006	0.003	0.025	0.007	0.002	0.017	0.181	0.338
Mg	0.109	0.416	0.171	0.508	0.170	1.000	1.197	0.990
Zn	0.725	0.408	0.207	0.387	0.599	0.203	0.504	1.512
Hercynite	21.08	22.43	64.14	15.57	28.80			
Galaxite	0.55	0.28	2.43	0.64	0.20			
Spinel	10.17	39.14	16.62	46.52	15.69			
Gahnite	68.09	38.21	20.12	35.44	55.31			

while that for the shorter 10 second count time shows a slightly broader range of 240 to 3240 ppm (Supplementary Appendix Table S2b). The Mn content reaches up to 0.34 wt.% Mn but is generally <0.2 wt.% Mn, while the Cu content is even lower (mostly <0.1 wt. Cu).

6. Geochemistry of various rocks in the Dawson-Green Mountain trend

6.a. Composition of granitoids in the Dawson area

Whole rock analyses of four types of granitoids (biotite-quartz monzodiorite/diorite, pink banded unit, leucogranite and alkali granite) adjacent to the Dawson deposit were done to evaluate chemical similarities and differences between the various rock types and to assist in determining their origin (Supplementary Appendix Tables S3a1, S3a2, S3a3, S3b, S3c, S3d1, S3d2). Although the Al₂O₃ concentrations overlap for the biotite-quartz monzodiorite/diorite (14.4 to 17.4 wt.% Al₂O₃) and the pink banded unit (11.4 to 15.1 wt.% Al₂O₃), these contents are generally higher than those for the alkali granite (12.6 to 13.4 wt.% Al₂O₃) and leucogranite (9.2 to 14.1 wt.% Al₂O₃). The silica contents for the last three granitoids range from 68.8 to 80.7 wt.% SiO₂, while those for biotite-quartz monzodiorite/monzonite range from 55.1 to 62.7 wt.% SiO₂. These concentrations, when combined with values of

total alkalis (Na₂O+K₂O = 3.6 to 6.6 wt.%), show that this granitoid falls in the monzodiorite and diorite fields, while the three other granitoids plot as granites (Fig. 12a). The monzodiorites/diorites have higher concentrations of Co, Cs, Ga, Nb, Ni, P₂O₅, Sc, TiO₂, V, Zn and Zr than the three types of granites (Supplementary Appendix Tables S3a1, S3a2, S3a3). Where the composition of the granitoids are plotted as CaO+Na₂O+K₂O vs SiO₂ the granites plot primarily in the calc-alkalic and calcic fields while most of the monzodiorites/diorites plot in the calc-alkalic field (Fig. 12b, f). These four granitoids can also be considered to be peraluminous ferroan granitoids as indicated in plots of FeO_{total}/(FeO_{total}+MgO) vs SiO₂ wt.% (Fig. 12b) and Al₂O₃/(Na₂O+K₂O) vs Al₂O₃/(CaO+Na₂O+K₂O; Fig. 12c). Plots of Ta vs Y, and Rb vs Y+Nb support the concept that these granitoids formed in a volcanic arc setting (Fig. 12d–f). Such a setting was proposed previously for the Paleoproterozoic granites in Colorado (e.g. Wobus *et al.* 2001).

Chondrite-normalized REE plots of the pink banded unit (Supplementary Appendix Fig. S1a) and monzodiorites/diorites (Supplementary Appendix Fig. S1b) show light rare earth element (LREE) enrichment, heavy rare earth element (HREE) depletion and negative Eu anomalies. The overall REE content is generally higher for monzodiorites/diorites compared to pink banded unit granitoids with the latter having flatter HREE signatures. Although leucogranites (Supplementary Appendix

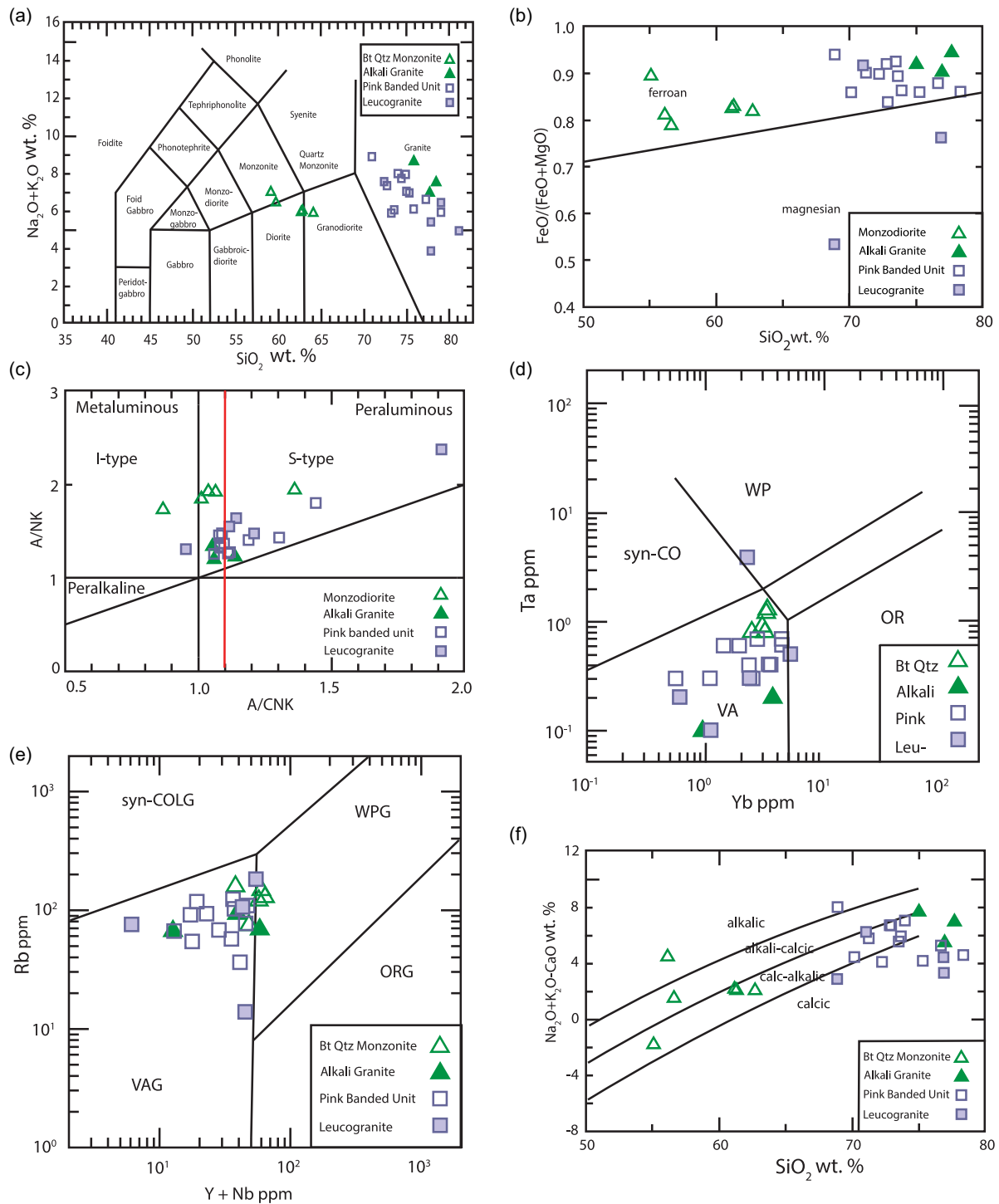


Figure 12. (Colour online) Discrimination diagrams of granitoids (biotite-quartz monzonite/diorite, alkali granite, pink banded unit and leucogranite) spatially related to the Dawson deposit. (a) Plot of $\text{Na}_2\text{O}+\text{K}_2\text{O}$ vs SiO_2 for intrusive rocks (after Le Bas *et al.*, 1986). (b) $\text{FeO}_{\text{total}}/(\text{FeO}_{\text{total}}+\text{MgO})$ vs SiO_2 weight % (after Frost & Frost (2011)). (c) A/NK $[\text{Al}_2\text{O}_3/(\text{Na}_2\text{O}+\text{K}_2\text{O})]_{\text{molar}}$ vs A/CNK $[\text{Al}_2\text{O}_3/(\text{CaO}+\text{Na}_2\text{O}+\text{K}_2\text{O})]_{\text{molar}}$ (after Maniar & Piccoli, 1989). (d) Ta vs Yb discrimination plot for syn-collision (syn-COLG), volcanic arc (VAG), within plate (WPG) and normal and anomalous ocean ridge (ORG) granites (after Pearce *et al.*, 1984). (e) Rb vs Y+Nb for the same granitoids in 10d. (f) $\text{Na}_2\text{O}+\text{K}_2\text{O}-\text{CaO}$ (so-called MALI index of Frost & Frost, 2008).

Fig. S1c) and alkali granites show LREE enrichment (Supplementary Appendix Fig. S1d), the HREE patterns are more complicated for these two types of granitoids as alkali granite samples TVD19-6 and TVD19-7 show arcuate HREE patterns (with negative Eu anomalies), while sample TVD19-3

shows a small positive Eu anomaly. All but one (TVD19-8) of the five leucogranite samples show positive Eu anomalies whereas samples WP27WR, WP28WR and WP30WR exhibit an increase in chondrite-normalized HREE patterns from Gd to Lu (Supplementary Appendix Fig. S1d).

6.b. Geochemistry of other least altered rocks in the Dawson-Green Mountain trend

In addition to granitoids spatially related to the Dawson deposit, various gneisses (quartz-K-feldspar-biotite gneiss from Cotopaxi, paragneiss from Dawson, Green Mountain and Horseshoe, orthogneiss from Green Mountain), quartz garnetite from Green Mountain, and amphibolite from Green Mountain and Dawson were also analysed (Supplementary Appendix Tables S3b, S3c, S3d1, S3d2).

The most common lithology adjacent to the Cotopaxi deposit is a rock that Salotti (1965) referred to as 'biotite gneiss' largely because biotite is the most common mafic mineral. However, the rock essentially consists of quartz, microcline and oligoclase with minor biotite, muscovite, garnet, titanite, gahnite, magnetite and zircon. The magnetite occurs as isolated subhedral to euhedral grains surrounded by a circular moat of feldspar. Whole rock composition of this rock shows that it contains 77 to 84 wt. SiO₂, 8 to 11 wt.% Al₂O₃ and 4 to 5 wt.% K₂O, with low amounts of Na₂O (0.3 to 1.7 wt%) and low total Fe₂O₃+MgO (2.12 to 3.73 wt%) (Supplementary Appendix Table 3b). The analysed rocks contain up to 469 ppm Cu, 46 ppm Pb and 1292 ppm Zn, the last of which reflects the presence of gahnite, and between 2131 and 4547 ppm Ba. Although it is likely this rock represents a metapelite, the other possibility is that the protolith consisted of volcanoclastics largely derived from a rhyolitic source rock (e.g. rhyolitic tuff). These two alternatives are hard to distinguish given the high metamorphic grade and the similarity of chondrite-normalized REE patterns (light HREE-enriched, HREE depletion and a negative Eu anomaly, Supplementary Appendix Fig. S2a) which are characteristic of both metamorphosed pelitic rocks (e.g. Slack & Stevens, 1994) and rhyolites (e.g. Streck, 2014).

The precursors to most of the gneisses from the Dawson and Green Mountain deposits is unclear due to the effects of metamorphism and the lack of volcanic features. Whether they are metasedimentary rocks or have an igneous origin is debatable. They vary from cordierite-plagioclase-quartz-biotite gneiss (TVD19-58), to more quartz-rich varieties that contain mostly garnet, biotite and sillimanite (TVD19-15, TVD19-81, AHCO-16). These rocks also contain trace magnetite-pyrite±pyrrhotite. The cordierite-rich gneiss (>70 cordierite) is silica-poor (52 wt.% SiO₂) and the most enriched in Fe₂O₃, MgO, Na₂O, K₂O, MnO, TiO₂, V and Rb, relative to the other three samples which contain between 71 and 87 wt.% SiO₂ (Supplementary Appendix Table S3b, Supplementary Appendix Fig. S2b). These four rocks contain between 106 and 845 ppm Ba, which is considerably less Ba than in the biotite gneiss from Cotopaxi. These rocks also contain 14 to 64 ppm Cu, 6 to 14 ppm Pb and 30 to 336 ppm Zn. Like the biotite gneiss from Cotopaxi, chondrite-normalized REE patterns for samples of gneisses from Dawson and Green Mountain are light HREE-enriched and HREE-depleted and show a negative Eu anomaly (Supplementary Appendix Fig. S2b).

A rock that is locally found in the Green Mountain and Dawson areas is a quartzo-feldspathic garnet-rich gneiss (Fig. 4i) that superficially resembles the so-called Potosi Gneiss intimately associated with the Broken Hill deposit, Australia, which Stevens & Barrons (2002) considered to be a metamorphosed rhyodacite. Two samples from Green Mountain contain 72 and 75 wt.% SiO₂, 11 and 13 wt.% Al₂O₃, 9 wt.% Fe₂O₃, <2 wt.% K₂O + Na₂O and 2 and 3 wt.% MgO (Supplementary Appendix Table S3b). Both samples are

also generally depleted in Cu (14 and 34 ppm), Pb (5 and 6 ppm) and Zn (39 and 80 ppm) and show LREE-enriched, HREE-depleted and prominent negative Eu anomalies chondrite-normalized REE patterns (Supplementary Appendix Fig. S2c).

Quartz-garnet rocks spatially associated with the Green Mountain deposit resemble exhalative quartz garnetites (meta-exhalites) spatially associated with metamorphosed massive sulphide deposits elsewhere in the world (e.g. Spry *et al.* 2000, 2007). The rocks at Green Mountain generally consist of garnet and quartz with minor to moderate amounts of biotite in some samples (Fig. 7a). The quartz to garnet ratio is generally high with garnet reaching up to 1 cm in diameter. These rocks contain 74 to 86 wt.% SiO₂, 5 to 10 wt.% Al₂O₃, 7 to 10 wt.% Fe₂O₃ generally <1 wt.% K₂O + Na₂O (0.3 to 1.7 wt.%) and 1 to 2 wt.% MgO (Supplementary Appendix Table S3c). They also contain up to 339 ppm Cu and 96 ppm Zn but are depleted in Pb (<4 ppm). Chondrite-normalized REE patterns for the quartz garnetites from Green Mountain are light HREE-depleted and HREE-enriched and show a negative Eu anomaly (Supplementary Appendix Fig. S2d).

At Green Mountain, garnet amphibolite is deformed and consists of coarse garnet (up to ~1 cm) in a matrix of plagioclase, hornblende, quartz and minor magnetite (Fig. 4h). However, there are also garnet-free amphibolites at Green Mountain and the Dawson deposit. For example, sample EHB-20-AMPH from Green Mountain contains the same minerals as the garnet amphibolite (minus garnet), but it also contains disseminated chalcopyrite, pyrite, and sphalerite within hornblende and along grain boundaries, which are the dominant metallic minerals in the deposit. These amphibolites contain 43 to 54 wt.% SiO₂, 11 to 16 wt.% Al₂O₃, 3 to 18 wt.% Fe₂O₃, 0.7 to 3.0 wt.% K₂O + Na₂O and 3 to 12 wt.% MgO (Supplementary Appendix Table S3c). Of note is that amphibolite from Green Mountain contains considerably higher concentrations of Fe₂O₃ (16 to 18 wt.%) than those from the Dawson deposit, which contain between 4 and 5 wt.% Fe₂O₃.

6.c. Geochemistry of metamorphosed altered rocks associated with mineralization

Samples of metamorphosed altered rocks, mainly gahnite-bearing, were collected from the El Plomo, Horseshoe, Cinderella, Cotopaxi and Green Mountain deposits to complement previous studies by Spry *et al.* (2022b) on nodular sillimanite rocks, which they considered to represent zones of metamorphosed hydrothermal alteration. In general, these gahnite-bearing altered rocks are dominated by orthoamphiboles and phlogopite, but they also contain various combinations of the following minerals: clinoamphibole, cordierite, quartz, chlorite, disseminated sulphides, chlorite, zircon, epidote and allanite. Chondrite-normalized REE plots of these rocks mostly show an enrichment in LREEs and flat HREEs with negative Eu anomalies (Supplementary Appendix Fig. S2f). The REE patterns resemble those for metasedimentary rocks (Supplementary Appendix Fig. S2b), quartzofeldspathic garnet-rich gneisses (Supplementary Appendix Fig. S2c) and amphibolites (Supplementary Appendix Fig. S2e). Sample TVD19-66 shows the lowest total amount of REEs and exhibits a weak positive Eu anomaly. It also contains the highest Ca content (23.6 wt.% CaO) and among the lowest concentrations of Fe (3.6 wt.% Fe₂O₃) of the metamorphosed altered rocks (Supplementary Appendix Table 3d2).

7. Sulphur isotope studies

7.a. Sampling methods and results

Samples were collected from drill core (Dawson, El Plomo), surface dumps (El Plomo, Horseshoe, Vulcan, Good Hope) and archive collections from the US Geological Survey (Copper King, Denver City), and museum collections of the Denver Museum of Nature and Science (Betty, Bon Ton, Sedalia, Cotopaxi). The sulphur isotope data are listed in Table 7 and shown in Fig. 13. Values of $\delta^{34}\text{S}$ ($n = 86$) of sulphides in different massive sulphide deposits in central-southern Colorado are generally similar and centred around 0–+2‰ with a range of $\delta^{34}\text{S} = -3.29$ to +6.45‰. Isotopic values for the individual minerals are $\delta^{34}\text{S} = -0.90$ to +6.45‰ for pyrite ($n = 56$), +2.51 to +3.83‰ for pyrrhotite ($n = 4$), -1.97 to +3.40‰ for chalcopyrite ($n = 5$), -3.29 to +5.85‰ for sphalerite ($n = 18$) and -0.90 to +1.16 for galena ($n = 3$). We have divided the isotopes into three geographic regions: western (Good Hope, Vulcan and Denver City), central (Betty, Bon Ton, Sedalia, Copper King and Cotopaxi) and eastern deposits (Dawson, El Plomo and Horseshoe). Values of $\delta^{34}\text{S}$ of -0.24 to +0.48‰ for pyrite from Good Hope ($n = 5$) are within the range of isotope values of -0.90 to +2.07‰ ($n = 20$) for pyrite from the Vulcan deposit. Single isotopic values for sphalerite and galena from the Vulcan deposit are -0.60‰ and +1.62‰, respectively, while sphalerite from the Denver City deposit ranges from -0.69 to +0.26‰ ($n = 3$). The eastern deposits generally exhibit higher $\delta^{34}\text{S}$ values than the western deposits: Dawson ($\delta^{34}\text{S} = +1.27$ to +3.69‰ for pyrite, $n = 6$; $\delta^{34}\text{S} = +3.27$ to +3.47‰ for pyrrhotite, $n = 2$); El Plomo ($\delta^{34}\text{S} = +1.12$ to +2.42‰ for pyrite, $n = 5$; $\delta^{34}\text{S} = +1.52$ to +1.76‰ for sphalerite, $n = 3$; $\delta^{34}\text{S} = -0.40$ ‰ for galena; $n = 1$); and Horseshoe ($\delta^{34}\text{S} = +0.77$ to +3.23‰ for pyrite, $n = 18$; $\delta^{34}\text{S} = +2.92$ to +3.40‰ for chalcopyrite, $n = 2$; $\delta^{34}\text{S} = +2.93$ ‰ for galena; $n = 1$). Sulphides from Cotopaxi mostly plot in the negative range ($\delta^{34}\text{S} = -3.29$ to -1.23‰, $n = 9$), with the one pyrite measurement plotting at a much higher, anomalous, positive value ($\delta^{34}\text{S} = +6.45$ ‰). In this context, it should be noted that G.T. Ririe (unpub. PhD thesis, Univ. Iowa, 1981) obtained five isotopic compositions of sulphides from Paleoproterozoic massive sulphide deposits in central Colorado with the lightest values also being from the Cotopaxi deposit ($\delta^{34}\text{S} = -4.4$ ‰ and -2.9‰ for galena and pyrite, respectively). The other three values obtained by G.T. Ririe (unpub. PhD thesis, Univ. Iowa, 1981) are $\delta^{34}\text{S} = +0.1$ ‰ for chalcopyrite from Green Mountain, -0.4‰ for pyrrhotite from an unidentified 'Grape Creek area mine', and +1.1‰ for pyrite from the Marion deposit in the southern Wet Mountains. The isotopic values obtained by him overlap those obtained in the present study.

8. Discussion

8.a. Comparison of metamorphosed massive sulphide deposits in Colorado

To see through the camouflaging effects of metamorphism and deformation, deposits in the Gunnison area are the best to evaluate the genesis of ore deposits as they were least deformed and subject to the lowest metamorphic grade. There are at least eight deposits in the Gunnison area (White Iron, Headlight, Anaconda, Ironcap, Good Hope-Vulcan, Midland, Denver City and Yukon). The Gunnison deposits occur in an east-west trending belt over a distance of ~50 km, with all but the Yukon deposit occurring in the Dubois Greenstone Belt. As pointed by Drobeck (1981) and

Sheridan *et al.* (1981), the deposits are hosted in metamorphosed bimodal felsic and mafic igneous rocks along with metamorphosed epiclastic and pyroclastic rocks and spatially related iron formation (e.g. Vulcan-Good Hope mine). Drobeck (1981) suggests the protoliths of the metamorphosed felsic rocks include rhyolite, quartz latite and dacite, while precursors to the mafic rocks were likely basalts and andesites (now hornblende schists and amphibolite). Although there are granitoids throughout the Dubois Greenstone Belt, they do not host sulphide mineralization. Instead, the deposits are elongate and commonly occur along the contacts between mafic and felsic igneous rocks.

In the Sedalia mine area, which was metamorphosed to lower amphibolite facies, bimodal mafic and felsic metavolcanic rocks (U-Pb age of 1728 ± 5 Ma, Boardman & Bickford, 1982) were identified by Boardman (1986) who described quartz-feldspar volcanoclastics, basaltic volcanics (basalt porphyry) and volcanoclastics, and slightly younger gabbro/diabase intrusive sheets. Phenocrysts and flattened pumice fragments occur in some rocks. A granite pluton (1671 ± 5 Ma, J. Hankins, unpub. BS thesis Carleton College, 1981) located ~7 km north of the Salida deposit is younger than the volcanoclastic rocks. The dominant rock type associated with the Sedalia deposit is feldspathic gneiss, which Sheridan and Raymond (1984b) suggested was originally flows or tuffs with the composition of rhyodacite. Garnet-cordierite-anthophyllite rocks are the most common host to mineralization. Of note is also the presence of porphyroblastic andalusite biotite-quartz gneiss/schist, in which the porphyroblasts of andalusite are up to 4 cm in length. This rock type may be the lower-metamorphic grade equivalent of nodular sillimanite rocks that Spry *et al.* (2022b) considered to be metamorphosed zones of hydrothermal alteration. Similar andalusite-rich rocks occur in the footwall alteration of the Kamantoo Cu deposit, South Australia (Pollock *et al.* 2018).

Despite the difficulties in separating primary geological features from features that are associated with the effects of metamorphism, the studies of, for example, Drobeck (1981), Sheridan and Raymond (1984a, 1984b) and Boardman (1986) show the presence of bimodal volcanic rocks spatially associated with mineralization in the lower grade metamorphic rocks. At higher metamorphic grades (upper amphibolite facies), the presence of primary volcanic textures is difficult or almost impossible to discern given the strong deformation that affected these rocks and the spatially related ore deposits. Despite the high proportion of granitoids in the vicinity of the Cotopaxi deposits and along the DGMT, these deposits occur in hydrothermally altered metasedimentary rocks (both clastic and likely volcanoclastic) and not in granitoids. Moreover, the genetic relationship to granitoids is speculative at best given there are no geochronological studies done on them in the DGMT. On the other hand, there is geochemical and textural evidence for the presence of amphibolite and gabbros in the sequence of rocks below the Dawson deposit, which was metamorphosed to the upper amphibolite facies, along with likely rhyodacites (i.e. precursors to the quartzo-feldspathic garnet-rich gneiss). Such rocks are also found adjacent to the Green Mountain deposit along with garnet amphibolite. The presence of visible sphalerite, chalcopyrite and pyrrhotite in metagabbro near Green Mountain raises the question as to whether sulphides were synchronous with the formation of the gabbro or whether the sulphides replaced it after the gabbro formed. Regardless, there is an intimate relationship among volcanic rocks, including volcanoclastic rocks, metamorphosed clastic rocks and sulphide mineralization in all the deposits studied here.

Table 7. Sulphur isotope compositions of sulphides from Proterozoic massive sulphide deposits, Colorado

Sample no.	Deposit	$\delta^{34}\text{S}$ per mil					Sample no.	Deposit	$\delta^{34}\text{S}$ per mil					
		Py	Po	Ccp	Sp	Gn			Py	Po	Ccp	Sp	Gn	
13674	Betty					-0.90	EHB21-032	El Plomo	+2.42					
13676	Betty			+0.71	+5.85		EHB21-033	El Plomo	+1.30					
S-58-75	Bon Ton				+2.88		EHB21-034	El Plomo				+1.52		
12687	Calumet (Salida)	+1.40					EHB21-036	El Plomo						-0.40
CK-18-08-226.5	Copper King			-0.86			9143c	Good Hope	-0.24					
13637	Cotopaxi				-2.51		EHB21-074	Good Hope	+0.10					
13638	Cotopaxi				-2.57		EHB21-075	Good Hope	+0.21					
13642	Cotopaxi				-3.26		EHB21-076	Good Hope	+0.48					
18134	Cotopaxi	+6.45			-3.29		EHB21-077	Good Hope	+0.44					
EHB-20-021	Cotopaxi				-2.50		EHB21-003	Horseshoe	+1.40					
EHB21-039	Cotopaxi				-1.23		EHB21-004	Horseshoe	+1.83			+2.93		
EHB21-040	Cotopaxi			-1.97	-2.11		EHB21-005	Horseshoe	+1.50					
EHB21-045	Cotopaxi				-1.62		EHB21-008	Horseshoe	+0.98					
DA-18-13-417.4	Dawson	+1.79					EHB21-011	Horseshoe	+2.08					
DA-18-15-839.5	Dawson	+1.27					EHB21-012	Horseshoe	+1.87					
DA-18-16-593.6	Dawson	+1.87					EHB21-013	Horseshoe	+2.50					
DA-18-16-663	Dawson	+1.35					EHB21-015	Horseshoe	+0.77					
TVD-64	Dawson	+2.64					EHB21-016	Horseshoe	+2.82					
TVD-73	Dawson	+3.69					EHB21-017	Horseshoe	+2.36					
TVD-74	Dawson		+3.47				EHB21-018	Horseshoe	+1.41					
TVD-76	Dawson		+3.27				EHB21-021	Horseshoe	+1.65					
S-30A-77	Denver City				+0.26		EHB21-022	Horseshoe	+0.77					
S-30C-77	Denver City				-0.69		TVD19-68a	Horseshoe	+1.84					
S-30D-77	Denver City				-0.24		TVD19-68c	Horseshoe	+2.21					
EHB21-023	El Plomo	+1.60					TVD19-69	Horseshoe	+3.00		+2.92			
EHB21-025	El Plomo	+2.06					TVD19-76	Horseshoe	+3.23					
EHB21-026	El Plomo	+1.12					TVD-19-72	Horseshoe	+2.53		+3.40			
EHB21-028	El Plomo				+1.54		TVD19-53	Horseshoe		+2.51				
EHB21-029	El Plomo				+1.76		TVD19-56	Horseshoe		+3.83				
EHB21-063	Vulcan	-0.46					V-1	Vulcan	+1.62					
EHB21-064	Vulcan	-0.54					V-2	Vulcan					+1.16	
EHB21-065	Vulcan	-0.77					V-3	Vulcan	+1.55					
EHB21-066	Vulcan	-0.40					V-4	Vulcan	+2.07					
EHB21-067	Vulcan	-0.29			-0.60		V-5	Vulcan	+1.70					
EHB21-068	Vulcan	-0.28					V-6	Vulcan	+1.74					
EHB21-069	Vulcan	-0.34					99CO-101	Vulcan	+1.50					
EHB21-070	Vulcan	-0.39					99CO-102	Vulcan	+1.62					
EHB21-071	Vulcan	-0.57					99CO-105	Vulcan	+1.42					
EHB21-072	Vulcan	-0.60					99CO-104	Vulcan	+1.74					
EHB21-073	Vulcan	-0.90												

Ccp, chalcocopyrite; Gn, galena; Po, pyrrhotite; Py, pyrite; Sp, sphalerite.

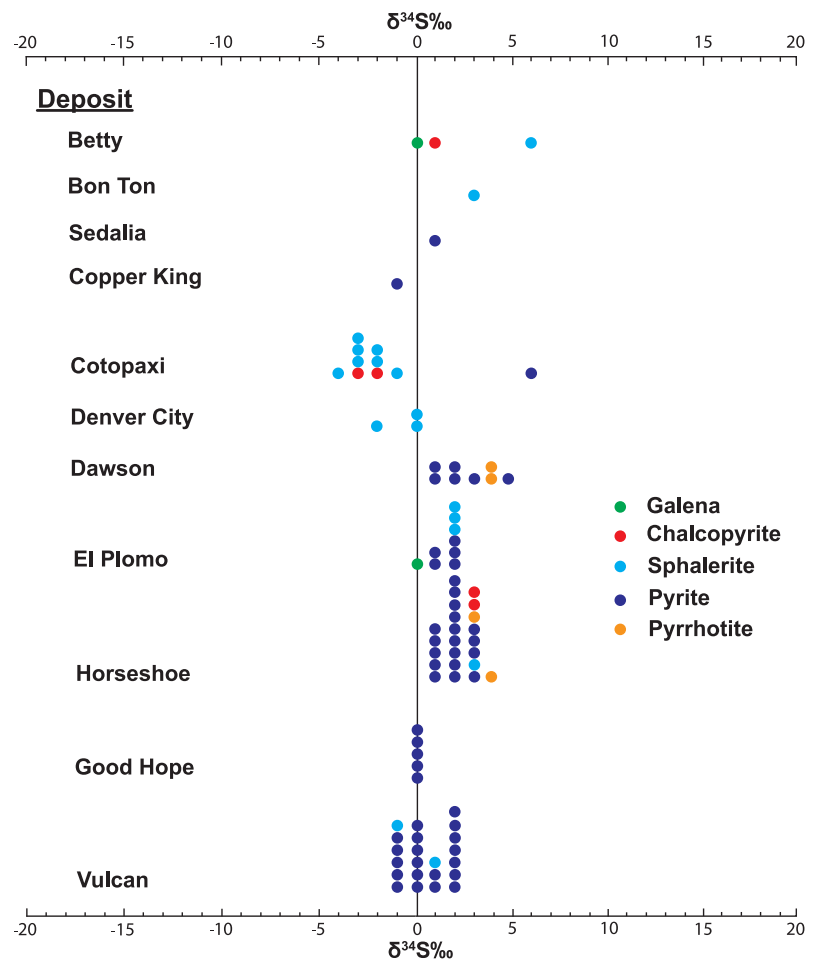


Figure 13. (Colour online) Sulphur isotopic compositions of sulphides (chalcopyrite, galena, pyrite, pyrrhotite and sphalerite) from metamorphosed massive sulphide deposits, Colorado.

8.b. Genesis of metamorphosed massive sulphide deposits in central Colorado compared to other massive sulphide deposits

The origin of massive sulphide deposits in Colorado is controversial with four genetic models having been proposed VMS (e.g. Drobeck, 1981; Sheridan & Raymond, 1984a), skarn (e.g. Salotti, 1965, Heinrich 1981), BHT (<https://www.zephyrminerals.com/el-plomo-section>) and peraluminous granitoids-hosted deposits (Kleinhans & Swan, 2022). In this evaluation, we address aspects that relate to the geological, mineralogical, and geochemical features identified here and data reported in previously published studies. These features are summarized in Table 8 and discussed below.

8.b.1 Skarn model

Heinrich (1981) recognized three types of sulphide deposits in metamorphic rocks in central Colorado, W, Cu-W, and Cu-Zn, and proposed that all three types are skarn deposits. The W and Cu-W deposits are primarily associated with meta-carbonate horizons with various combinations of the following minerals: vesuvianite, grossular, diopside, epidote, scapolite, tremolite, calcite, titanite, zoisite and clinozoisite (among others) forming the skarn assemblage. However, the Cu-Zn deposits studied by Heinrich (1981) and here contain sphalerite and/or gahnite, and nearly all deposits are not hosted in metamorphosed calcite/

dolomite horizons or calc-silicate gneisses, exceptions being three small Cu-Zn±Pb occurrences (Cresswell, Hosa Lodge, F.M.D.) in Jefferson County that occur in calc-silicate-quartz-microcline biotite gneiss (Eckel, 1997). Gahnite at the Creswell mine occurs sillimanite-rutile-topaz-rich gneiss, which is a likely exhalative unit and not a skarn (Marsh & Sheridan, 1976; Heimann *et al.* 2006). Furthermore, Salotti (1965) in identifying the Cotopaxi deposit as a skarn deposit noted that the sulphide mineralization is hosted in amphibolite. However, the amphibolite Salotti (1965) described consists of anthophyllite-cordierite-biotite-gahnite±clinohumite ±garnet±diopside alteration. Other minor hornblende-plagioclase amphibolites occur in the vicinity of the deposit but do not host ore. Salotti (1965) also pointed out that the granite spatially associated with the Cotopaxi deposit is post-mineralization and is a 'typical Pikes Peak granite' which formed around 1.1 Ga. There is no granite genetically related to the mineralization, and there are no typical endoskarms or exoskarms spatially related to the massive sulphides.

8.b.2 Granite-hosted model

Kleinhans and Swan (2022) recently proposed that the Cu-Zn±Pb deposits are high-temperature hydrothermalite fractionates of granitoid intrusive rocks and further argued that such a model was also responsible for the formation of the Broken Hill Pb-Zn-Ag deposit, Australia. Geochemical studies here support the idea of Kleinhans and Swan (2022) that peraluminous granites are

Table 8. Comparison of Paleoproterozoic deposits in Colorado with VMS, BHT, Skarn, and PISZHG deposits*

	Deposit type				
	Colorado	VMS	Skarn	BHT	PISZHG
Spatial relationship of deposits to granitoids	✓	X✓	✓	X✓	✓
Genetic relationship of deposits to granitoids	X	X	✓	X	✓
Back-arc rift on continental crust or intracontinental rift	✓	X✓	✓	✓	✓
Spatial relationship to non-granitoid intrusive rocks including mafic rocks	✓	✓	X	✓	X
Spatial relationship to exhalative or inhalative rocks†	✓	✓X	X	✓	X
Cu-Zn±Pb±Ag-dominated ore systems	✓	✓	✓	X	X
Ore hosted in metasediments	✓	X✓	X	✓X	X
Mineralization spatially related to shear zones	X✓	✓X	✓X	✓	✓
Spatial relationship to Mg alteration	✓	✓X	X	X	X
Gedrite/anthophyllite-cordierite-gahnite-biotite ±garnet alteration assemblage	✓	✓	X	X	X
Metamorphosed from greenschist to granulite facies	✓	✓	X	✓	?
Presence of gahnite and hōgbomite in ore zones	✓	X✓	X	X	X
Small range in sulphur isotope compositions centred near δ 34 S = 0‰	✓	✓	✓	✓	✓

*VMS, volcanogenic massive sulphide, BHT, Broken Hill type; PISZG, peraluminous-intrusive shear zone-hosted gold.

†Iron formation, quartz garnetite, and quartz-gahnite rocks.

✓ = yes; X = no; ✓X = most commonly yes but no at some deposits; X✓ = most commonly no but yes in some deposits.

spatially associated with the Dawson deposit, but they state that the sulphide mineralization is hosted by a biotite aplite. This terminology has genetic implications, since an aplite is a fine-grained igneous rock primarily composed of quartz, alkali feldspar, and plagioclase with small amounts of muscovite and biotite. Instead, the so-called aplite they identified is a sheared anthophyllite-biotite-garnet-cordierite-feldspar gahnite rock. Such a rock resembles metamorphosed altered rocks spatially associated with all the massive sulphide deposits studied here that were metamorphosed to the upper amphibolite facies. Moreover, Cu-Zn deposits in Colorado occur in metasedimentary and metavolcanic rocks and not in granitoids. Accordingly, the granite-related hydrothermalite model of Kleinhans and Swan (2022) is tenuous at best, especially when the ages of the granitoids spatially

related to the Dawson deposit, which was the focus of their study, are unknown. Furthermore, the granitoids spatially related to the Sedalia and the Cotopaxi deposit are younger than the sulphide mineralization, which further supports the concept that sulphide mineralization is genetically unrelated to the formation of granitoids (Salotti, 1965; Sheridan & Raymond, 1984b).

In supporting their genetic model, Kleinhans and Swan (2022) suggested that the giant BHT Pb-Zn-Ag deposit was an example of a high-temperature hydrothermalite fractionate that formed from granitoids. Peraluminous granites occur in the Willyama Supergroup that hosts the Broken Hill Pb-Zn-Ag deposit with the peraluminous Rasp Ridge Granite Gneiss having the same age as the mineralization. However, this metamorphosed granitoid, which is a quartz-K feldspar-plagioclase-biotite gneiss, occurs stratigraphically below the deposit and contains no sulphide mineralization (Page *et al.* 2005). Instead, sulphide mineralization occurs in metasedimentary rocks associated with the Hores Gneiss, a regionally extensive, metamorphosed volcanoclastic unit that is stratigraphically equivalent to the orebody. The immediate host to ore is the Potosi Gneiss, a garnet-biotite-rich quartzofeldspathic gneiss that has a rhyodacite composition, which contains volcanic quartz and feldspar phenocrysts, and rip-up clasts of sediment (Stevens & Barrons, 2002). Therefore, there is no evidence that the Broken Hill deposit formed from magmato-hydrothermal, high-temperature hydrothermalites. Their proposal also does not recognize the fact that there are hundreds of small BHT Pb-Zn deposits in the Willyama Supergroup that show no spatial relationship to granitoids.

8.b.3. Broken Hill-type (BHT) model

BHT deposits are among the largest metamorphosed massive sulphide deposits in the world with Broken Hill, Australia, being the biggest and Cannington being one of the highest grade silver deposits (38 Mt @ 500g/t Ag, 11.1% Pb and 4.4% Zn). Spry and Teale (2021) suggested the major characteristics of BHT deposit are: 1. high Pb+Zn+Ag values, 2. metamorphosed from greenschist to granulite facies, 3. sulphur-poor mineralogy (e.g. gahnite, plumbian feldspar, löllingite, pyrrhotite rather than pyrite); 4. a spatial association of sulphides to bimodal (felsic and mafic) volcanic rocks, oxidized metasedimentary rocks, and stratabound gahnite- and garnet-bearing rocks and iron formations; 5. stacked orebodies with characteristic Pb:Zn:Ag ratios and skarn-like Fe-Mn-Ca-F gangue assemblages, and the presence of minor Cu, Au, Bi, As, and Sb; 6. restriction of deposits to rocks of 1.70 to 1.67 Ga age within the Diamantina Orogen; 7. spatial association to continental rifts; and 8. no genetic relationship to granitoids. Of the metamorphosed massive sulphide deposits in Colorado only the Green Mountain and El Plomo deposits share some characteristics with BHT deposits, but they also show significant differences. Like BHT deposits, Green Mountain is spatially associated with iron formation, gahnite-rich rocks, quartz garnetite, garnet amphibolite and a garnet-biotite-rich quartzofeldspathic gneiss, the last of which shows mineralogical and geochemical characteristics that resemble the Potosi Gneiss at Broken Hill. REE patterns for the quartz garnetite at Green Mountain contrasts to quartz garnetites from elsewhere in the world including Broken Hill, which are light HREE-enriched and HREE-depleted (e.g. Spry *et al.* 2000). Instead, the patterns of quartz garnet rocks from Green Mountain (see Supplementary Appendix Fig. S2d) more closely resemble the chondrite-normalized patterns of individual garnet analyses reported in the literature (e.g. Lottermoser, 1988; Schwandt *et al.* 1993; Spry

et al. 2000). This is likely due to garnet essentially contributing nearly all of the REEs to the whole rock composition with quartz and other minor to trace minerals providing only a small contribution.

Garnet amphibolite from Green Mountain was analysed because it mineralogically and texturally resembles garnet amphibolite spatially associated with the Broken Hill deposit, Australia (e.g. Raveggi *et al.* 2007) and the King Zn VMS deposit, Western Australia (Hollis *et al.* 2019). The high Fe₂O₃ and TiO₂ concentrations suggest that these rocks are ferrobasalts that were recognized previously by Byerly *et al.* (1976) from the Galapagos spreading centre. They are rare in nature but characteristic of the so-called high Fe-Ti basaltic rocks (now garnet amphibolite) associated with the Broken Hill deposit. The REE patterns of garnet-amphibolite from Green Mountain and Dawson show slightly enriched HREEs and slightly depleted LREEs with moderate to prominent negative Eu anomalies, which are similar to those from Broken Hill (Supplementary Appendix Fig. S2e).

However, important differences show that Green Mountain is a Cu-Zn deposit with only minor Pb and Ag values, and it does not show stacked orebodies or skarn-like Fe-Mn-Ca-F gangue assemblages. Instead, sulphide mineralization at Green Mountain is hosted in anthophyllite-cordierite-gahnite-almandine garnet altered rocks. Like El Plomo and other massive sulphide deposits in Colorado, Green Mountain formed in a volcanic arc setting rather than being associated with continental rifting. Although there is uncertainty with the age of sulphide mineralization in Colorado, Pb-Pb isotope ages (Sheridan & Raymond 1984a, 1984b) suggest that sulphide mineralization is older (1.8–1.7 Ga) than BHT deposits in the Diamantina Orogen (Stevens *et al.* 2008). In evaluating the prospectivity of the DGMT for BHT deposits, Zephyr Minerals (<https://www.zephyrminerals.com/el-plomo-section>) proposed that there was base metal zoning along the DGMT with El Plomo prospect showing high grades of Pb, Zn, and Ag in drill holes GC-8 and GC-9. For example, drill hole GC-9 contains up to 10.2% Zn, 0.03% Pb, and 5.9 g/t Ag, over 2.5 m and 0.02% Zn, 2.61% Pb, and 179 g/t Ag, over 0.7 m (unpub. Report to US Borax, 1981). While the Ag and Zn grades rival those of Broken Hill, they are over intersections of <3 m with the high Ag grades correlating with the higher grades of Pb. The deposits are dominated by pyrite and pyrrhotite rather than sphalerite and galena. Furthermore, El Plomo shows no stacked orebodies and is not spatially associated with Fe-Mn-Ca-F gangue. Instead sulphide mineralization primarily occurs in anthophyllite-cordierite-gahnite-almandine garnet altered rocks similar to those associated with other massive sulphide deposits metamorphosed to the upper amphibolite facies elsewhere (e.g. Montauban, Quebec, Bernier *et al.* 1987; Geco, Ontario, Zaleski *et al.* 1991; King, Western Australia, Hollis *et al.* 2019). While some deposits along the DGMT show some geological characteristics similar to BHT deposits, including sulphur isotope compositions of sulphides centred on 0 per mil, nearly all other deposits in Colorado including Dawson and Horseshoe along the DGMT show little resemblance to BHT deposits (Spry *et al.* 2021).

8.b.4. Volcanogenic massive sulphide model

The geochemical, mineralogical and geochemical features for deposits in Colorado given in Table 8 are most supportive of a VMS model. Such features include: 1. the spatial association of sulphides with bimodal felsic and mafic igneous rocks within packages of metasedimentary/metavolcaniclastic rocks. Although best observed in the least metamorphosed massive sulphide districts

(Gunnison (upper greenschist–lower amphibolite facies) and in the vicinity of the Sedalia district (lower amphibolite facies), such rocks also host mineralization metamorphosed to the upper amphibolite facies, even where the local terrane (e.g. Dawson) is dominated by granitoids. For example, meta-amphibolites and metagabbros are commonly associated with mineralization along with the presence of garnet-biotite-rich quartzofeldspathic gneiss that are likely metarhyodacites. 2. Sulphide mineralization is commonly associated with nodular sillimanite rocks (andalusite-rich rocks at the Sedalia deposit) or anthophyllite/gedrite-cordierite-biotite-garnet-gahnite rocks both of which are zones of metamorphosed hydrothermal alteration (e.g. Spry *et al.* 2022b). Deposits in the Gunnison area are spatially associated with quartz-muscovite±carbonate (e.g. Denver City) or chlorite-muscovite alteration (e.g. Ironcap, Vulcan). Orthoamphibole-cordierite rocks generally result from a reaction between chlorite and muscovite which is a common assemblage in the alteration zones of deposits in the lower grade Gunnison district. Note there is no evidence of footwall stockwork alteration zones below deposits, instead the alteration appears to be more stratabound similar to that associated with the Scuddles VMS deposit, Australia (Large, 1992). 3. A spatial association of some deposits to meta-exhalite/meta-inhalites of Spry *et al.* (2000). Such rocks include iron formation (e.g. Vulcan-Good Hope, Green Mountain, Dawson), gahnite-bearing schists (e.g. Sedalia), quartz-garnetite (Green Mountain) and sulphide-bearing metachert (e.g. Gunnison district). 4. Stratiform nature of massive sulphide horizons (e.g. Dawson). 5. At Dawson, sulphide mineralization is hosted in metasedimentary/metavolcaniclastic rocks, which occur as inclusions in granitoids. This implies these rocks and contained mineralization are older than the granitoids.

The presence of elevated concentrations of accessory elements such as Au, Ag, As, Bi, Hg, Sb, Se, and Te at Vulcan-Good Hope, Au, Ag, Bi, As, and Sb at Green Mountain, and Au, Bi, Se, and Te at Dawson are not unusual for VMS deposits (e.g. Barrie & Hannington, 1999). In the Good-Hope and Dawson systems, minerals containing these elements cross-cut earlier formed massive sulphides, while Au, Ag, Bi, As and Sb are elevated in the massive sulphide horizon at Green Mountain. Although Drobeck (1981) raised the possibility that veins containing minerals in the system Au-Ag-Te-Se at Vulcan-Good Hope may be Miocene in age (although the age of the mineralization is unknown), Kleinhans and Swan (2022) show that the Au-Te-Se-Bi assemblage at Dawson is associated with pink peraluminous granite, implying that these elements are Proterozoic in age, similar to that of the base metal mineralization. Given that Au, Ag, Bi, As and Sb are elevated in the highly deformed massive sulphides at Green Mountain begs the question as to whether these trace elements, along with the presence of minerals in the system Bi-Se-Te-S at Dawson, were the products of remobilization of the massive sulphides rather than being derived from the peraluminous granite. It should be noted that while this zone of bonanza gold in this assemblage parallels the massive sulphide at Dawson, it also occurs in contact with it locally. Evidence for the remobilization of gold in metamorphosed VMS deposits was reported previously from the Mobern Cu-Zn (Larocque *et al.* 1995), Boliden Au-Cu-As (Wagner *et al.* 2007) and Falun Zn-Pb-Cu-(Au-Ag) deposits (Kampmann *et al.* 2018). Of particular relevance is that the Falun deposit is spatially associated with various cordierite-anthophyllite altered rocks and that remobilization of the massive sulphides generated quartz veins containing elevated concentrations of Pb, Bi, Se and Au and the presence of Pb-Bi sulphosalts and native

gold. These elements were likely liberated from pyrite (Kampmann *et al.* 2018). The association of cordierite-anthophyllite rocks to sulphide mineralization at Dawson and Green Mountain, the dominance of pyrite as the sulphide in both deposits and the presence of a trace element signature similar to that observed at Falun suggest that pyrite was also the likely host to these elements in the Colorado deposits. Similarly, such a liberation of trace elements from pyrite to generate elevated Au, Ag, As, Bi, Hg, Sb, Se and Te contents in cross-cutting quartz veins in Vulcan-Good Hope deposit is also likely.

One aspect of the deposits in the Grape Creek-Dawson trend is the spatial association with a deformation zone (the so-called Dawson shear zone of Kleinhans & Swan, 2022), which runs through or parallel to several deposits. The brecciated nature of the ore at Dawson, for example, implies that the ore was present prior to shearing. The question remains whether the location of the deformation zone which primarily occurs in the metasedimentary/metavolcaniclastic rocks is due to a competency contrast between the more easily deformed metasedimentary/metavolcaniclastic rocks and the surrounding granitoids, which dominate the lithologies between El Plomo and Dawson. The more than 30 minor prospects along the linear trend may simply be reflecting multiple hydrothermal vent sites as opposed to being derived from magmatic-hydrothermal fluids in a later formed shear zone.

The alteration box plot of Large *et al.* (2001) has been applied here to samples from the deposits with the aim of seeing through the camouflaging effects of metamorphism to identify the nature and intensity of the precursor alteration (Fig. 14). The box plot has been used previously to evaluate hydrothermal alteration associated with metamorphosed and relatively unmetamorphosed massive sulphide deposits (e.g. Theart *et al.* 2010, Frank *et al.* 2019, Hollis *et al.* 2019). The chlorite-carbonate-pyrite index (CCPI = $100(\text{MgO} + \text{FeO}_{\text{total}}) / (\text{MgO} + \text{FeO}_{\text{total}} + \text{Na}_2\text{O} + \text{K}_2\text{O})$) of Large *et al.* (2001) is plotted against the Ishikawa alteration index (AI = $[100(\text{MgO} + \text{K}_2\text{O}) / (\text{MgO} + \text{K}_2\text{O} + \text{Na}_2\text{O} + \text{CaO})]$) with the least altered volcanic rocks plotting towards the centre of the diagram. Assuming a spatial relationship of mineralization to volcanic rocks, which was noted previously, samples from Green Mountain and Cotopaxi suggest the precursor alteration minerals were chlorite, sericite and pyrite. Such an alteration assemblage also likely affected the garnet-bearing quartzo-feldspathic gneisses from Green Mountain. Precursors to altered rocks from Horseshoe and Cinderella most probably contained chlorite, and sericite, while meta-amphibolite were likely weakly to moderately altered basaltic/andesitic rocks. Such a precursor assemblage is commonly associated with VMS deposits.

The relatively narrow range of sulphur isotopic compositions ($\delta^{34}\text{S} = -3.3$ to $+6.5\text{‰}$) for the metamorphosed massive sulphide deposits in Colorado (Fig. 13), which is centred around $+1\text{‰}$ suggests a magmatic contribution of sulphur to the deposits. Although it should be noted here that such an isotopic range does not preclude the previously mentioned genetic models, we suggest here that sulphur was likely leached from precursor clastic sedimentary or volcanoclastic piles. Metasedimentary/metavolcaniclastic rocks are free of organic material (i.e. graphite) suggesting that isotopic fractionation was not the result of bacteriogenic sulphate reduction. Instead, thermochemical sulphate reduction (TSR) is the most likely cause of the isotopic fractionation assuming equilibrium among the sulphides (pyrite, pyrrhotite, chalcopyrite and locally galena). It is also a reasonable assumption that sulphides were in equilibrium prior to metamorphism since

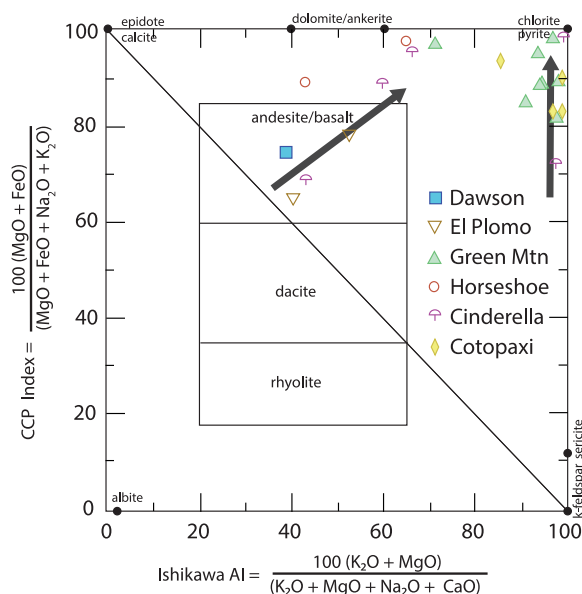


Figure 14. (Colour online) Chlorite-carbonate-pyrite index (CCPI) vs Ishikawa alteration index (AI) alteration box plot of Large *et al.* (2001) for samples from the Dawson-Green Mountain trend (modified after Large *et al.* 2001). Central box indicates least altered samples for felsic, intermediate and mafic rocks, while the arrows show the alteration trend.

banded sulphides in metamorphosed ore deposits at, for example, Vulcan are probably the result of syngenetic processes rather than due to metamorphism or deformation (Dudley & Bruekner, 2022). Isotopic variations are likely due to small differences in physicochemical conditions (i.e. T , $f\text{O}_2$, pH, ionic concentration of the ore fluid (I) and $\delta^{34}\text{S}_{\text{SS}}$; Ohmoto, 1972), rather than to differences in lithological composition. Due to the effects of metamorphism, the T , $f\text{O}_2$, pH, I and $\delta^{34}\text{S}_{\text{SS}}$ of the pre-metamorphic ore-forming hydrothermal fluid can only be estimated. Based on the mineralogy of the ore and the likely precursors to the metamorphosed altered rocks, some approximations can be made when considering the systems Cu-Fe-S-O and K-Al-Si-O-H, which are relevant to the massive sulphide systems in Colorado. Based on the solubility of chalcopyrite and its common presence in nearly all of the massive sulphide deposits, we assume a minimum temperature of the ore fluid of $\sim 270^\circ\text{C}$ (e.g. Large, 1992). The presence of the alteration assemblages muscovite-quartz-pyrite and chlorite-muscovite quartz at Vulcan, along with precursors to the alteration assemblage gedrite/anthophyllite-cordierite-bearing rocks at most deposits, suggests that, based on the system K-Al-Si-O-H, the ore fluid is largely confined to the muscovite stability field. Pyrite-pyrrhotite is the most common assemblage in the system Fe-S-O with pyrite-pyrrhotite-magnetite being present in some deposits (e.g. Dawson, Green Mountain, El Plomo). In a plot of $\log f\text{O}_2$ -pH (Fig. 15), the sulphur isotope compositions for pyrite (given that it is the most common sulphide analysed herein) overlap the stability fields of muscovite, pyrite-pyrrhotite and pyrite-pyrrhotite-magnetite would require $T = \sim 350^\circ\text{C}$, $I = \sim 1$ m NaCl (approximate seawater salinity), a total dissolved S content of ~ 0.1 moles/kg H_2O and $\delta^{34}\text{S}_{\text{SS}} = +1\text{‰}$. Varying these parameters significantly does not allow an overlap between the sulphur isotope compositions with the aforementioned stability fields. For example, if it is assumed that the S in solution was derived from the isotopic

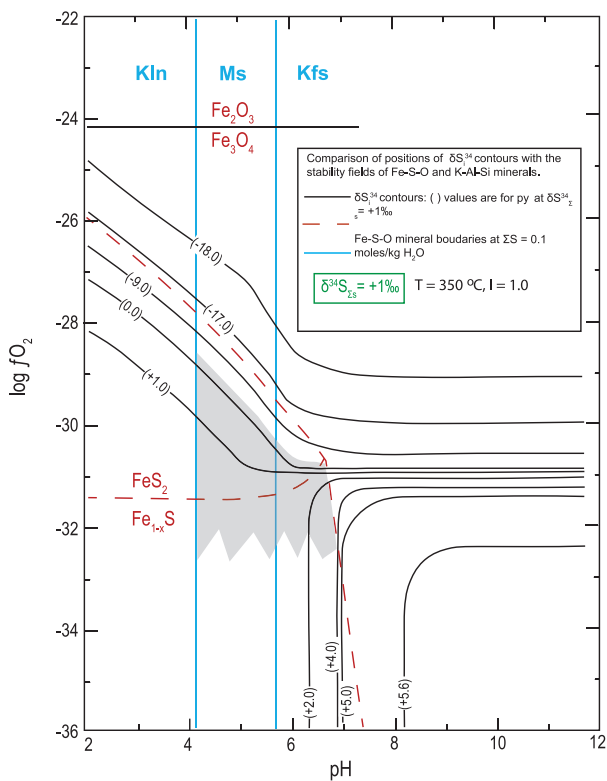


Figure 15. (Colour online) A $\log f_{\text{O}_2}$ -pH diagram for massive sulphides from Colorado. Sulphur isotope contours for sphalerite are drawn for $\delta^{34}\text{S} = +1\text{‰}$ and $T = 350\text{ °C}$. Minerals in the system Fe-S-O are shown for $\Sigma\text{S} = 0.1$ moles/kg H_2O as red dashed lines. The shaded region shows the approximate range of conditions for $\delta^{34}\text{S}$ of sphalerite over f_{O_2} -pH range indicated (primarily along the pyrrhotite-magnetite join. Note that the shaded area starts at the pyrite-magnetite-pyrrhotite triple point to accommodate the rare presence of primary pyrite. Modified after Ohmoto (1972).

reduction of sulphate in the global ocean, which at around that time (i.e. ~ 1.8 to 1.7 Ga), was $\delta^{34}\text{S} = \sim 20\text{‰}$ (Canfield & Farquar, 2009), or that the ore-forming fluid had a $T < 300\text{ °C}$, the sulphur isotope values observed here for pyrite do not overlap the stability fields of muscovite and members of the system Fe-S-O. The assumptions made here are approximate at best and do not allow for changes as fluid temperatures decreased or the likely possibility of some interaction of the hydrothermal fluid with seawater. The most likely source of sulphur are the volcanic rocks (either mafic or felsic or both) with possible leaching of sulphur from the spatially associated sedimentary/volcaniclastic rocks surrounding the deposits.

As a further attempt to determine the genesis of the deposits, we evaluated the Zn/Cd ratios of sphalerite. Wen *et al.* (2016) proposed that the composition of sphalerite can be used as a way to classify different types of Pb-Zn deposits and pointed out that the Cd content of sphalerite is dependent on T , pH, the nature and concentration of ligands in the ore fluid that bonds to Zn and Cd, and the total sulphur in solution. Wen *et al.* classified Pb-Zn deposits into three groups: low temperature (i.e. MVT deposits), high temperature (i.e. porphyry, magmatic-hydrothermal, skarn and VMS deposits) and exhalative systems (i.e. Sedex and seafloor hydrothermal sulphides). The classification scheme was based on Cd concentrations and Zn/Cd ratios in sphalerite as well as a plot of Cd isotopes vs. Zn/Cd ratios. Although the metamorphosed massive sulphide deposits studied here are mostly Cu-Zn deposits, galena is a minor sulphide in nearly all deposits and is common in

the El Plomo deposit and locally in the Cinderella deposit. While Zn/Cd ratios have been used in the classification of Pb-Zn deposits by Wen *et al.* (2016), the Zn/Cd ratios of sphalerite in the Vulcan, Horseshoe, El Plomo and Dawson deposits fall within the overlap region of VMS and Sedex deposits identified by Spry *et al.* (2022a) (Supplementary Appendix Fig. S3, Supplementary Table Appendix S2a). The reason for this is unclear. However, it may be reflecting both VMS and Sedex characteristics since the VMS deposits are hosted in metasedimentary/metavolcaniclastic rocks.

8.c. Exploration guides to metamorphosed massive sulphide deposits in Colorado

Previous studies by Spry and Scott (1986), Spry and Petersen (1989), Heimann *et al.* (2005), and Spry *et al.* (2000, 2022a) show that the presence of iron formations, nodular sillimanite rocks, orthoamphibole-cordierite-bearing rocks, quartz garnetite, and gahnite- and h ogbomite-bearing rocks can be used as potential exploration guides to metamorphosed massive sulphide deposits. Willner *et al.* (1990) also considered that topaz- and rutile-bearing gneisses can be used as exploration guides to sulphide deposits. Such rocks were identified by Heimann *et al.* (2006) in the Evergreen area (along with orthoamphibole-cordierite garnet rocks) and elsewhere in Colorado by Marsh & Sheridan (1976), Fisher *et al.* (2022) and Kleinhans *et al.* (2022). All of these rocks have been observed in Colorado and serve as pathfinders to ore. Moreover, the composition of zincian spinels and zincian h ogbomite have compositions that are compatible with these minerals having formed by desulphidation reactions in most locations supporting the concept that their presence may be indicative of nearby sulphides (see Spry, 2000; Heimann *et al.* 2005).

9. Conclusions

The main conclusions of the present study are as follows:

1. Semimassive to massive sulphide deposits in central Colorado occur in a volcanic arc setting that were subsequently metamorphosed anywhere from the upper greenschist to upper amphibolite-granulite facies. They likely formed around 1.8 to 1.7 Ga. Our preferred genetic model is for the deposits to be VMS deposits with bimodal-mafic deposits occurring in the Gunnison area and mafic-siliclastic deposits dominating other locations in Colorado including the DGMT. This is due to the dominance of felsic and mafic igneous rocks at Gunnison and the presence of metamorphosed volcaniclastic rocks with a predominance of metamafic intrusive rocks (amphibolite and gabbro) associated with other deposits. There appears to be no genetic relationship of sulphide deposits to granitoids even though they are spatially related to most deposits.
2. Although Zn/Cd ratios of sphalerite do not distinguish among the previously proposed genetic models, sulphur isotope compositions are consistent with a magmatic source of sulphur that reflects TSR, rather than biogenic reduction processes. These isotopic compositions, when coupled with the nature of the precursor minerals in the metamorphosed altered rocks and gangue minerals, along with those in the system Fe-S-O, suggest the following approximate conditions of ore formation: $T = \sim 350\text{ °C}$, $I = \sim 1$ m NaCl, a total dissolved S content of ~ 0.1 moles/kg H_2O and $\delta^{34}\text{S}_{\Sigma\text{S}} = +1\text{‰}$.

3. Zincian spinels occur in various rock types in Colorado including non-sulphide bearing metasiliclastic and metavolcaniclastic rocks, but they are mostly found in sulphide-bearing metamorphosed altered rocks or in sulphide-rich assemblages. The new data obtained here are consistent with the highly variable compositions reported previously by Heimann *et al.* (2005) from other deposits in Colorado. Where the sulphide-bearing metamorphosed altered rock contains a paucity of magnesian silicates, the spinel is dominated by the gahnite molecule, which is dictated by temperature and the buffering capacity of sphalerite and Fe sulphides. However, where the rock contains an abundance of Mg-rich silicates (e.g. biotite, ortho- and calcic-amphiboles, chlorite, cordierite) and disseminated sulphides, the composition of the zincian spinel has a higher proportion of spinel *sensu stricto* molecule since the Mg component of zincian spinels is not buffered by fS_2 .
4. The distribution of nodular sillimanite rocks, gahnite-bearing rocks and rutile-topaz rocks constitutes zones of metamorphosed stratabound hydrothermal alteration, while iron formations and quartz garnetite serve as exhalites/inhalites. They, along with metamorphosed altered rocks dominated by orthoamphiboles, cordierite and gahnite±högbomite, serve as exploration guides to metamorphosed massive sulphide deposits in Colorado and elsewhere in the world.

Supplementary material. The supplementary material for this article can be found at <https://doi.org/10.1017/S0016756823000407>

Acknowledgements. This study was financially supported by Zephyr Minerals and by grants to EB from the Rocky Mountains Association of Geologists Foundation and the Society of Economic Geologists Foundation. Discussions with Will Felderhoff, Mark Graves and Loren Komperdo of Zephyr Minerals along with Trevor Van Dyke, Stan Keith and Monte Swan about the geology of the Dawson-El Plomo-Green Mountain deposits, are greatly appreciated. Evelyne Leduc (QFIR) is thanked for providing sulphur isotope standards, while James Hagadorn and Nicole Neu-Yagle (Denver Museum of Nature and Science) and Karen Kelley (US Geological Survey) kindly provided samples for the sulphur isotope study. Justin Glenn assisted with drafting of some figures. The reviews of Bertus Smith and an anonymous reviewer are greatly appreciated and improved the quality of the manuscript. Tim Johnson is also thanked for his comments and editorial handling of the paper.

References

- Alers B and Shallow JM** (1996) Semiconformable Cu–Zn, Zn–Pb–Ag, synvolcanic mineralization and rhyolitic volcanic successions in polydeformed terranes of the Proterozoic Colorado Province. *Geological Society of America Abstracts with Programs* **28**, A-155.
- Anderson JL and Cullers RL** (1999) Paleo- and Mesoproterozoic granite plutonism of Colorado and Wyoming. *Rocky Mountain Geology* **34**, 149–64.
- Armbruster T** (2002) Revised nomenclature of högbomite, nigerite, and taaffeite minerals. *European Journal of Mineralogy* **14**, 389–95.
- Barrie CT and Hannington MD** (1999) Classification of volcanic-associated massive sulfide deposits based on host-rock composition. *Reviews in Economic Geology* **8**, 1–11.
- Bennett VC and DePaolo DJ** (1987) Proterozoic crustal history of the western United States as determined by neodymium isotopic mapping. *Geological Society of America Bulletin* **99**, 674–85.
- Berke EH, Spry PG, Heimann A, Teale GS, Johnson B, Von der Handt A, Alers B and Shallow JM** (2022) The genesis of metamorphosed Paleoproterozoic massive sulfide occurrences in central Colorado: geological, mineralogical and sulfur isotope constraints. *Geological Society of America Abstracts with Programs*, **54**, 219. doi: [10.1130/abs/2022AM-378319](https://doi.org/10.1130/abs/2022AM-378319).
- Bernier L, Pouliot G and MacLean WH** (1987) Geology and metamorphism of the Montauban North Gold Zone: a metamorphosed polymetallic exhalative deposit, Grenville Province, Quebec. *Economic Geology* **82**, 2076–90.
- Bickford ME, Cullers RL, Shuster RD, Premo RL and Van Schmus WR** (1989) U–Pb zircon geochronology of Proterozoic and Cambrian plutons in the Wet Mountains and southern Front Range. In *Proterozoic Geology of the Southern Rocky Mountains* (eds JA Grambling and BJ Tewksbury), pp. 49–64. Denver, CO: Geological Society of America Special Paper 235.
- Boardman SJ** (1986) Early Proterozoic bimodal volcanic rocks in central Colorado, U.S.A., Part I: petrography, stratigraphy and depositional history. *Precambrian Research* **34**, 1–36.
- Boardman SJ and Bickford ME** (1982) U–Pb geochronology and petrology of Proterozoic volcanic and plutonic rocks in central Colorado. *Geological Society of America Abstracts with Programs* **14**, 448.
- Both RA and Stumpfl EF** (1987) Distribution of silver in the Broken Hill orebody. *Economic Geology* **82**, 1037–43.
- Burrett C and Berry R** (2000) Proterozoic Australia–Western United States (AUSWUS) fit between Laurentia and Australia. *Geology* **28**, 103–6.
- Byerly GR, Melson WG and Vogt PR** (1976) Rhyodacites, andesites, ferrobasalts and ocean tholeiites from the Galapagos spreading center. *Earth and Planetary Science Letters* **30**, 215–21.
- Cameron EN and Threadgold IM** (1961) Vulcanite, a new copper telluride from Colorado. *American Mineralogist* **46**, 258–68.
- Canfield DE and Farquar J** (2009) Animal evolution, bioturbation, and the sulfate concentration of the oceans. *Proceedings of the National Academy of Sciences* **106**, 8123–7.
- Chantler C, Olsen K, Dragoset R, Kishore A, Kotochigova S and Zucker D** (2005) X-ray form factor, attenuation and scattering tables (version 2.0). National Institute of Standards and Technology Standard Reference Database 66.
- Condie KC** (1982) Plate-tectonic model for Proterozoic continental accretion in the southwestern United States. *Geology* **10**, 37–42.
- Donnelly ME, Conway CM and Earhart RE** (1987) Records of massive sulfide occurrences in Arizona. *U.S. Geological Survey Open File Report* **87-0406**, 43.
- Donovan JJ, Singer JW and Armstrong JT** (2016) A new EPMA method for fast trace element analysis in simple matrices. *American Mineralogist* **101**, 1839–53.
- Donovan JJ and Tingle TN** (1996) An improved mean atomic number background correction for quantitative microanalysis. *Journal of the Microscopy Society of America* **2**, 1–7.
- Drobeck PA** (1981) Proterozoic syngenetic massive sulfide deposits in the Gunnison gold belt, Colorado. In *Western Slope (Western Colorado)* (eds RC Epis and JF Callender), pp. 279–86. Socorro, NM: New Mexico Geological Society 32nd Annual Fall Field Conference Guidebook.
- Dudley B and Bruekner SM** (2022) *The Origin of Pyrite-Sphalerite Banding in Metamorphosed Volcanogenic Massive Sulfide Deposits* (ed AB Christie), p. 49. 16th Biennial SGA Meeting, The Critical Role of Minerals in the Carbon-Neutral Future, March 28–31 2022, Rotorua, New Zealand, Abstracts 2.
- Eckel EB** (1961) Minerals of Colorado: A 100-year record. *United States Geological Survey Bulletin* **1114**, 399.
- Eckel EB** (1997) *Minerals of Colorado*. Golden, CO: Fulcrum Publishing, 665 p.
- Feenstra A** (1997) Zincohögbomite and gahnite in a diaspore-bearing metabauxite from eastern Samos (Greece): mineral chemistry, element partitioning and reaction relations. *Schweizerische Mineralogische und Petrographische Mitteilungen* **77**, 73–93.
- Fisher L, Kleinhans L and Fisher TR** (2022) Recent insights into Colorado central Front Range (CCFR) Tectonics and metallogeny. *Geological Society of America Abstracts with Programs* **54**, 219.
- Frank KS, Spry PG, Raat H, Allen RL, Jansson NF and Ripa M** (2019) Variability in the geological, mineralogical, and geochemical characteristics of base metal sulfide deposits in the Stollberg ore field, Bergslagen, Sweden. *Economic Geology* **114**, 473–512.
- Frost CD and Frost RB** (2011) On ferroan (S-type) granitoids: their compositional variability and modes of origin. *Journal of Petrology* **52**, 39–53.
- Frost RB and Frost CD** (2008) A geochemical classification for feldspathic igneous rocks. *Journal of Petrology* **49**, 1955–69.

- Gable DJ and Sims PK** (1969) Geology and regional metamorphism of some high-grade cordierite gneisses, Front Range, Colorado. *Geological Society of America Special Paper* **128**, 87 p.
- Gibson H, Lafrance B, Pehrsson S, DeWolfe M, Gilmore K, Simard R-L and Pearson B** (2013) Structural evolution of the Paleoproterozoic Flin Flon mining district, Manitoba: The anatomy of a giant VMS system. Manitoba Geological Survey Open File OF2013-6, 47 p.
- Grambling TA, Holland M, Karlstrom KE, Gehrels GE and Pecha M** (2015) Revised location for the Yavapai-Mazatzal crustal province boundary in New Mexico: Hf isotopic data from Proterozoic rocks of the Nacimiento Mountains. *New Mexico Geological Society Guidebook, 66th Field Conference, Geology of the Meadowlands, Las Vegas Region*, 175–84.
- Grassineau NV** (2006) High-precision EA-IRMS analysis of S and C isotopes in geological materials. *Applied Geochemistry* **21**, 756–65.
- Grew E, Hiroi Y and Shiraishi K** (1990) Högbomite from the Prince Olav Coast, East Antarctica: an example of oxidation-exsolution of a complex magnetite solid solution? *American Mineralogist* **75**, 589–600.
- Hartley TD** (1983). *Geology and Mineralization of the Vulcan-Good Hope Massive Sulfide Deposit*. Gunnison County, CO. Handfield, R.C., editor, *Gunnison Gold Belt and Powderhorn Carbonatite Field Trip Guidebook*: (ed RC Handfield). pp. 19–27. Denver Regional Exploration Geology Society.
- Hedge CE** (1970) Whole-rock age of the Pikes Peak batholith, Colorado. *US Geological Survey Professional Paper* **700-B**, B86–9.
- Heimann A, Spry PG and Teale GS** (2005) Zinc-rich spinels associated with Proterozoic base metal sulfide occurrences, Colorado, and their use as guides to metamorphosed massive sulfide deposits. *Canadian Mineralogist* **43**, 601–22.
- Heimann A, Spry PG, Teale GS and Jacobson CE** (2006) Coronas, symplectite textures, and reactions involving aluminous minerals in gedrite-cordierite gneisses from Evergreen, Front Range, Colorado. *Canadian Mineralogist* **44**, 1025–44.
- Heinrich EW and Griffiths WR** (1948) Turret corundum deposits, Chaffee County, Colorado. *American Mineralogist* **33**, 199.
- Heinrich EWM** (1981) Precambrian tungsten and copper-zinc skarn deposits of south-central Colorado. *Colorado Geological Survey Resource Series* **21**, 115 p.
- Hollis SP, Podmore D, James M, Doran A, Menuge JF, Yeats CJ and Wyche S** (2019) VHMS mineralisation at Erayinia in the Eastern Goldfields Superterrane: geology and geochemistry of the metamorphosed King Zn deposit. *Australian Journal of Earth Sciences* **66**, 135–81.
- Hutchison MN and Scott SD** (1981) Sphalerite geobarometry in the Cu-Fe-Zn-S system. *Economic Geology* **76**, 143–53.
- Jones JV III, Siddoway CS and Connelly JN** (2010) Characteristics and implications of ca.1.5 Ga deformation across a Proterozoic mid-crustal section, Wet Mountains, Colorado, USA. *Lithosphere* **2**, 119–35.
- Kampmann TC, Jansson NF, Stephens MB, Olin PH, Gilbert S and Wanheiman C** (2018) Syn-tectonic sulphide remobilization and trace element redistribution at the Falun pyritic Zn-Pb-Cu-(Au-Ag) sulphide deposit, Bergslagen, Sweden. *Ore Geology Reviews* **96**, 48–71.
- Karlstrom KE** (1998) Introduction to special issues: lithospheric structure and evolution of the Rocky Mountains (Parts I and II). *Rocky Mountain Geology* **33**, 157–9.
- Karlstrom KE, Harlan SS, Williams ML, McLelland J, Geissman JW and Ahall K-I** (1999) Refining Rodinia: geologic evidence for the Australia-western U.S. connection in the Proterozoic: *GSA Today* **9**, 1–7.
- Karlstrom KE and Humphreys G** (1998) Influence of Proterozoic accretionary boundaries in the tectonic evolution of western North America: interaction of cratonic grain and mantle modification events. *Rocky Mountain Geology* **33**, 161–79.
- Kleinbans L, Alers B, James LP, Piper JR and Fisher L** (2022) Three Precambrian zircon spinel occurrences in central Colorado Front Range (CCFR): characteristics and relationships potentially bearing on their genesis and metallogeny. *Geological Society of America Abstracts with Program* **54**, 219. doi: [10.1130/abs/2022AM-383515](https://doi.org/10.1130/abs/2022AM-383515).
- Kleinbans L and Swan M** (2022) Geological, geochemical, and geophysical characterization of gold in the Dawson peraluminous intrusive-related shear zone gold system, central Colorado. *Geological Society of America Abstracts with Program* **54**, 216.
- Large RR** (1992) Australian volcanic-hosted massive sulfide deposits: Features, styles and genetic models. *Economic Geology* **87**, 471–510.
- Large RR, Gemmell JB, Paulick H and Huston DL** (2001) The alteration box plot: a simple approach to understanding the relationship between alteration mineralogy and litho-geochemistry associated with volcanic-hosted massive sulfide deposits. *Economic Geology* **96**, 957–71.
- Larocque AC, Hodgson CJ, Carbri LJ and Jackman JA** (1995) Ion-microprobe analysis of pyrite, chalcopyrite and pyrrhotite from the Mobern VMS deposit in northwestern Quebec: evidence for metamorphic remobilization of gold. *Canadian Mineralogist* **33**, 373–88.
- Le Bas MJ, Le Maitre RW, Steckeisen A and Zanettin B** (1986) A chemical classification of volcanic rocks based on the total alkali-silica diagram. *Journal of Petrology* **27**, 745–50.
- Lindgren W** (1908) Notes on copper deposits in Chaffee, Fremont, and Jefferson counties, Colorado. *United Geological Survey Bulletin* **691**, 57–174.
- Lottermoser BG** (1988) Rare earth element composition of garnets from the Broken Hill Pb-Zn-Ag orebodies, Australia. *Neues Jahrbuch für Mineralogie Monatshefte* **9**, 423–31.
- Maniar PD and Piccoli PM** (1989) Tectonic discrimination of granitoids. *Geological Society of America Bulletin* **101**, 5635–43.
- Marsh SP and Sheridan DM** (1976) Rutile in Precambrian sillimanite-quartz gneiss and related rocks, East-Central Front Range, Colorado. Geology and resources of titanium in the United States. *United States Geological Survey Professional Paper* **959-G**, 17 p.
- Mishra B and Bernhardt H-J** (2009) Metamorphism, graphite crystallinity, and sulfide anatexis of the Rampura-Agucha massive sulfide deposit, northwestern India. *Mineralium Deposita* **44**, 183–204.
- Moleski N, Boxleiter A and Thakurta J** (2019) Sulfur isotope ratios from VMS deposits in the Penokean Volcanic Belt, Great Lakes Region, USA: constraints on the source of sulfur in a Paleoproterozoic intra-arc rift. *Minerals* **9**, 6. doi: [10.3390/min9010006](https://doi.org/10.3390/min9010006).
- Möller A, Berndt T, Walker D and Kelly NM** (2022) Monazite and garnet U-Pb dating reveals amphibolite facies metamorphism in central Colorado as Mesoproterozoic. *Geological Society of America Abstracts with Program* **54**, 219.
- Ockenga E, Yalçın Ü, Medenbach O and Schreyer W** (1998) Zincohögbomite, a new mineral from eastern Aegean metabauxites. *European Journal of Mineralogy* **10**, 1361–6.
- Ohmoto H** (1972) Systematics of sulfur and carbon isotopes in hydrothermal ore deposits. *Economic Geology* **67**, 551–78.
- Owens BE, Belkin HE and Zerolis JM** (2013) Margarite, corundum, gahnite and zincohögbomite in a blackwall, Raleigh Terrane, Eastern Piedmont Province, USA. *Mineralogical Magazine* **77**, 2913–29.
- Page RW, Stevens BPJ and Gibson GM** (2005) Geochronology of the sequence hosting the Broken Hill Pb-Zn-Ag orebody, Australia. *Economic Geology* **100**, 631–61.
- Parr JM and Plimer IR** (1993) Models for Broken Hill-type lead-zinc-silver deposits. In *Mineral Deposit Modeling* (eds RV Kirkham, WD Sinclair, RI Thorpe and JM Duke), pp. 253–88. Stittsville, ON: Geological Association of Canada Special Paper 40.
- Pearce JA, Harris NBW and Tindle AG** (1984) Trace element discrimination diagrams for the tectonic interpretation of granitic rocks. *Journal of Petrology* **25**, 956–83.
- Pedrick JN, Karlstrom KE and Bowring SA** (1998) Reconciliation of conflicting tectonic models for Proterozoic rocks of northern New Mexico. *Journal of Metamorphic Petrology* **16**, 687–707.
- Peterman ZE, Hedge CE and Braddock WA** (1968) Age of Precambrian events in the northeastern Front Range, Colorado. *Journal of Geophysical Research* **73**, 2277–96.
- Pollock MV, Spry PG, Tott KA, Koenig A, Both RA and Ogierman JA** (2018) The origin of the sediment-hosted Kanmantoo Cu-Au deposit, South Australia: mineralogical considerations. *Ore Geology Reviews* **95**, 94–117.
- Premo WR and Fanning CM** (2000) SHRIMP U-Pb zircon ages for Big Creek gneiss, Wyoming and Boulder Creek batholith, Colorado: implications for timing of Paleoproterozoic accretion of the northern Colorado province. *Rocky Mountain Geology* **35**, 31–50.
- Rakotonandrasana NOT, Arima M, Miyawaki R and Rambelson RA** (2010) Widespread occurrences of högbomite-2N2S in UHT metapelites from the

- Betroka belt, southern Madagascar: implications of melt or fluid activity during regional metamorphism. *Journal of Petrology* **51**, 869–95.
- Raveggi M, Giles D, Foden J and Raetz M** (2007) High Fe–Ti mafic magmatism and tectonic setting of the Paleoproterozoic Broken Hill Block, NSW, Australia. *Precambrian Research* **156**, 55–84.
- Raymond WH, Leiggi PA and Sheridan DM** (1980) Sapphirine in Precambrian rocks associated with stratabound massive sulfide deposits, Custer County, Colorado. *U.S. Geological Survey Bulletin* **1513**, 22 p.
- Rosenberg JL, Spry PG, Jacobson CE and Vokes FM** (2000) An evaluation of metamorphic sulfidation and oxidation reactions in and adjacent to the Bleikvassli Zn–Pb–(Cu) deposit, Nordland, Norway. *Mineralium Deposita* **35**, 714–26.
- Salotti CA** (1965) Mineralogy and paragenesis of the Cotopaxi, Colorado, Cu–Zn skarn deposit. *American Mineralogist* **50**, 1179–212.
- Schwandt CS, Papike JJ, Shearer CK and Brearley AJ** (1993) Crystal chemical control of REE incorporation in garnets from the Broken Hill Pb–Zn–Ag orebodies, Australia. *Canadian Mineralogist* **31**, 371–9.
- Shallow JM and Alers B** (1996) Metamorphic lithologies of a volcanogenic massive sulfide (VMS) hydrothermal system in the Proterozoic rocks of the Copper Gulch area, Fremont County, Colorado. *Geological Society of America Abstracts with Programs* **28**, A-155.
- Shaw CA and Karlstrom KE** (1999) The Yavapai–Mazatzal crustal boundary in the southern Rocky Mountains. *Rocky Mountain Geology* **34**, 37–52.
- Sheridan DM and Raymond WH** (1984a) Precambrian deposits of zinc–copper–lead sulfides and zinc spinel (gahnite) in Colorado. *U.S. Geological Survey Bulletin* **1550**, 31 p.
- Sheridan DM and Raymond WH** (1984b) Preliminary report on the geology of the Sedalia mine area and its Proterozoic deposits of base–metal sulfides and gahnite, Chaffee County, Colorado. *U.S. Geological Survey Open-File Report* **84-0800**, 27 p.
- Sheridan DM, Raymond WH and Cox LJ** (1981) Precambrian sulfide deposits in the Gunnison region, Colorado. In *Western Slope (Western Colorado)* (eds RC Epis and JF Callender), pp. 273–277. Socorro, NM: New Mexico Geological Society 32nd Annual Fall Field Conference Guidebook.
- Siddoway CS, Givot RM, Bodle CD and Heizler MT** (2000) Dynamic versus anorogenic setting for Mesoproterozoic plutonism in the Wet Mountains, Colorado: does the interpretation depend on level of exposure? *Rocky Mountain Geology* **35**, 91–111.
- Sims PK and Stein HJ** (2003) Tectonic evolution of the Proterozoic Colorado province, southern Rocky Mountains. *Rocky Mountain Geology* **38**, 183–204.
- Slack JF and Stevens BPJ** (1994) Clastic metasediments of the Early Proterozoic Broken Hill Group, New South Wales, Australia: geochemistry, provenance, and metallogenic significance. *Geochimica et Cosmochimica Acta* **58**, 3633–52.
- Spry PG** (2000) Sulfidation and oxidation haloes as guides in the exploration for metamorphosed massive sulfide deposits. *Reviews in Economic Geology* **11**, 149–61.
- Spry PG, Heimann A, Messerly J and Houk RS** (2007) Discrimination of metamorphic and metasomatic processes at the Broken Hill Pb–Zn–Ag deposit, Australia: rare earth element signatures of garnet-rich rocks. *Economic Geology* **102**, 471–94.
- Spry PG, Mathur RD, Teale GS and Godfrey LV** (2022a) Zinc, sulfur and cadmium isotopes and Zn/Cd ratios as indicators of the origin of the supergiant Broken Hill Pb–Zn–Ag deposit and other Broken Hill-type deposits, New South Wales, Australia. *Geological Magazine*. doi: [10.1017/S0016756822000590](https://doi.org/10.1017/S0016756822000590).
- Spry PG, McFadden S, Teale GS, Alers B, Shallow JM and Glenn JM** (2022b) Nodular sillimanite rocks as field indicators to metamorphosed massive sulfide deposits. *Ore Geology Reviews* **141**, 104632.
- Spry PG, Peters J and Slack JF** (2000) Meta-exhalites as exploration guides to metamorphosed ore. *Reviews in Economic Geology* **11**, 163–201.
- Spry PG and Petersen EU** (1989) Zincian högbomite as an exploration guide to metamorphosed massive sulfide deposits. *Mineralogical Magazine* **53**, 263–9.
- Spry PG and Scott SD** (1986) The stability, synthesis, origin and exploration significance of zincian spinels. *Economic Geology* **81**, 1446–1463.
- Spry PG and Teale GS** (2021) A classification of Broken Hill-type deposits: a critical review. *Ore Geology Reviews* **139**, 103935.
- Stensrud HL and More SW** (1980) Precambrian geology and massive sulfide environments of the west-central Haulapal Mountains, Mohave County, Arizona a preliminary report. *Arizona Geological Society Digest* **12**, 155–65.
- Stevens BPJ and Barrons IM** (2002) Volcanic textures in the Palaeoproterozoic Hores Gneiss, Broken Hill, Australia. *Geological Survey of New South Wales Quarterly Notes* **113**, 1–22.
- Stevens BPJ, Page RW and Crooks A** (2008) Geochronology of Willyama Supergroup metavolcanics, metasediments and contemporaneous intrusions, Broken Hill, Australia. *Australian Journal of Earth Sciences* **55**, 301–30.
- Strech MJ** (2014) Evaluation of crystal mush extraction models to explain crystal-poor rhyolites. *Journal of Volcanology and Geothermal Research* **284**, 79–94.
- Teale GS** (1980) The occurrence of högbomite and taaffeite in a spinel–phlogopite schist from the Mount Painter Province of South Australia. *Mineralogical Magazine* **43**, 575–7.
- Theart HFJ, Ghavami-Riabi R, Mouri H and Gräser P** (2010) Applying the box plot to the recognition of footwall alteration zones related to VMS deposits in a high-grade metamorphic terrain, South Africa, a litho-geochemical exploration application. *Chemie der Erde* **71**, 143–54.
- Tiu G, Jansson N, Wanhainen, Ghorbani Y and Lilja L** (2021) Ore mineralogy and trace element (re)distribution at the metamorphosed Lappberget Zn–Pb–Ag–(Cu–Au) deposit, Garpenberg, Sweden. *Ore Geology Reviews* **135**, 10423.
- Valley JW, Petersen E, Essene EJ and Bowman JR** (1982) Fluorophlogopite and fluortremolite in Adirondack marbles and calculated C–O–H–F fluid compositions. *American Mineralogist* **67**, 545–57.
- Van Alstine RE** (1969) Geology and mineral deposits of the Poncha Springs NE Quadrangle, Chaffee County, Colorado. *United States Geological Survey Professional Paper* **626**, 52 p.
- Wagner T, Klemm R, Wenzel T and Mattsson B** (2007) Gold upgrading in metamorphosed massive sulfide ore deposits: direct evidence from laser-ablation–inductively coupled plasma–mass spectrometry analysis of invisible gold. *Geology* **35**, 775–8.
- Warr L** (2021) IMA–CNMNC approved mineral symbols. *Mineralogical Magazine* **85**, 291–320.
- Wen H, Zhu C, Zhang Y, Cloquet C, Fan H and Fu S** (2016) Zn/Cd ratios and cadmium isotope evidence for the classification of lead–zinc deposits. *Nature Scientific Reports* **6**, 25273.
- Whitmeyer SJ and Karlstrom E** (2007) Tectonic model for the Proterozoic growth of North America. *Geosphere* **3**, 220–59.
- Willner AP, Schreyer W and Moore JM** (1990) Peraluminous metamorphic rocks from the Namaqualand Metamorphic Complex (South Africa): geochemical evidence for an exhalation-related, sedimentary origin in a Mid-Proterozoic rift system. *Chemical Geology* **81**, 221–40.
- Wobus RA, Folley MJ, Wearn KM and Noblett JB** (2001) Geochemistry and tectonic setting of Paleoproterozoic metavolcanics of the southern Front Range, lower Arkansas River and northern Wet Mountains, central Colorado. *Rocky Mountain Geology* **36**, 99–118.
- Yalçin Ü, Schreyer W and Medenbach O** (1993) Zn-rich högbomite formed from gahnite in the metabauxites of the Menderes Massif, SW Turkey. *Contributions to Mineralogy and Petrology* **113**, 314–24.
- Zaleski E, Froese E and Gordon TM** (1991) Metamorphic petrology of Fe–Zn–Mg–Al alteration at the Linda volcanogenic massive sulfide deposit, Snow Lake, Manitoba. *Canadian Mineralogist* **29**, 995–1017.